Université Grenoble Alpes

Master Thesis

for the degree of

Master in Environmental Fluid Mechanics

LABORATOIRE DES ECOULEMENTS GEOPHYSIQUES ET INDUSTRIELS

A climatological study of heat waves in Grenoble over the 21st century

Author: Francisco AMARAL[a,b]

First Supervisor: Prof. Chantal STAQUET[a,b]

Second Supervisor: Dr. Sara BACER[a,b]

[a] *Université Grenoble Alpes, Grenoble, France*

[b] *Laboratoire des Écoulements Géophysiques et Industriels (LEGI), Grenoble, France*

KEYWORDS

Regional climate change

Heat waves

Grenoble valley

Climate data analysis

ABSTRACT

We investigate heat waves (HWs) affecting the valley of Grenoble in a future climate. In this study, heat waves are defined as periods of at least 3 consecutive days of daily maximum and minimum temperature exceeding the 92nd historical percentile. This definition has been chosen to select HWs that might impact human health. Even though only the strongest HWs are potentialy harmful, the definition allows to identify a sufficient number of events to perform a statistical study. The HWs are characterised by their duration, peak temperature and mean daily maximum temperature. Additionally, each HW is studied per year using a framework measuring heat wave number, duration, participating days, and the peak and mean magnitudes. The HW characteristics are calculated with the results of simulations from the regional climate model MAR. MAR was forced by reanalysis and by a global model for the entire 21st century. The uncertainty of future anthropogenic forcing is taken into account by analysing results for the shared socio-economic pathways SSP2 and SSP5. The simulations are evaluated against in-situ measurements in the past period. MAR captures well daily maximum and minimum temperatures as well as observed HWs. Under future climate conditions, the increase in very hot daily maximum and minimum temperatures is mainly due to the shift rather than the broadening of their probability density functions. Additionally, the HWs become more frequent and have a longer duration, higher peak temperature and mean daily maximum temperature. Finally, a sensitivity analysis to the HW defining threshold is carried out.

Submission date: January 25, 2022

financé par IDEX Université Grenoble Alpes

Contents

Chapter 1

Introduction

The global average temperature has increased by 0.89°C since 1900, with most of the warming due to anthropogenic activity (Hartmann et al. 2013). Climate science literature discusses extensively that small changes in average temperature can result in disproportionally larger changes in the intensity and frequency of extremes (Mearns et al. 1984; Boer et al. 2001). For a given climatological period (i.e. a period of at least 30 years), the probability density function (PDF) of air temperature is a Gaussian curve with center at the mean value, μ, and standard deviation, σ, representing its variability. For the same σ, an increase in the mean of the temperature PDF yields higher frequencies of hot weather, as well as hot extremes that were rare in the original PDF. An increase in σ only results in the broadening of the PDF which results in a higher probability of extremes in both hot and cold weather. A shift in mean temperature and an increase in σ are reported to be occurring (Perkins 2015), thus having a combined influence on the increase of hot temperature extremes. Changes in observed temperature extremes have been detected since the turn of the millennium (e.g. Easterling et al. 2000), though with regional variations. Further research is required to understand the relationship between changes in the temperature PDF and changes in temperature extremes at the regional and local scale. This thesis proposes a local study focused on a particular type of temperature extreme - heatwaves (HWs). The temporal evolution of the main HW characteristics will be investigated during the 21st century.

Heatwaves are known to be associated with increased daily mortality (Pascal et al. 2006) and thus, have impacts on human health. The effects of extreme hot temperature are mostly severe when there is a lack of relief between hot days (Pezza et al. 2012). A number of major heat wave events occurred over the past decade, many of which had devastating health effects (D'Ippoliti et al. 2010). In 2003, a mega heatwave occurred over Western Europe and was responsible for over 70,000 deaths (Coumou et al. 2013). In this study, we focus on HWs in connection with their potential human health impacts.

There is no standardized definition of a heat wave. In the human health sector, the existing definitions generally refer to a summer period of at least 3 consecutive days during which the daily maximum and minimum air temperatures are above a certain threshold. We use a percentile-based approach to define this threshold, making it dependant on the considered climatological period. Further details on the HW definition are given in section 2.2. Additionally, we propose a sensitivity analysis of this threshold in section 3.3.

Previous studies have investigated the changes of European HW characteristics at a regional scale. Given their impacts on health, it is of interest to study HWs in areas of high population density. We focus our study at the scale of an urban area namely, in the valley of Grenoble in the Alps region. The measurements and the model data describing air temperature in Grenoble and used in this study are presented in section 2.1.

The main objective of this thesis is to study the evolution of HW characteristics over this

century and, thus, to address the local impact of climate change on HW events. This is done for the summer period in the valley of Grenoble. For this study, a regional climate model (RCM) forced by reanalysis and by a global climate model (GCM) is used. The climatological period 1985-2014 is used as reference to benchmark extreme events in the future. In chapter 2, we compare the RCM forced by reanalysis against observations. Then, the percentile threshold for HWs will be defined and evaluated. This is followed by the definition of HW characteristics which allow to compare and quantify different HW events. In chapter 3, the results are put forward and discussed. As a first step, the RCM forced by the GCM is evaluated. Then, the characteristics of future heat waves are analysed. Additionally, a sensitivity analysis is carried out for the threshold which defines a HW. Finally, conclusions are drawn and future progress in the topic is proposed in chapter 4.

Chapter 2

Data and heat wave definition

In this chapter, we present the data used in this study, consisting in field measurements and model data. Additionally, the models under scope will be briefly presented. Then, the definition of heat wave and heat wave characteristics will follow. Only summer heat waves are studied where summer is defined as the months of May, June, July, August, September and October (MJJASO months hereon).

2.1 Data

2.1.1 In-situ measurements

A data set of observations for the period 1985-2014 was provided by ATMO-AURA[1], the air quality agency for the Auvergne-Rhône-Alpes region. This data set consists of hourly in-situ measurements of air temperature at 2m above the ground for the MJJASO months. These observations were taken at the Pont de Claix (PodC) weather station located in the south of the valley of Grenoble at an altitude of 237 meters (figure 2.1).

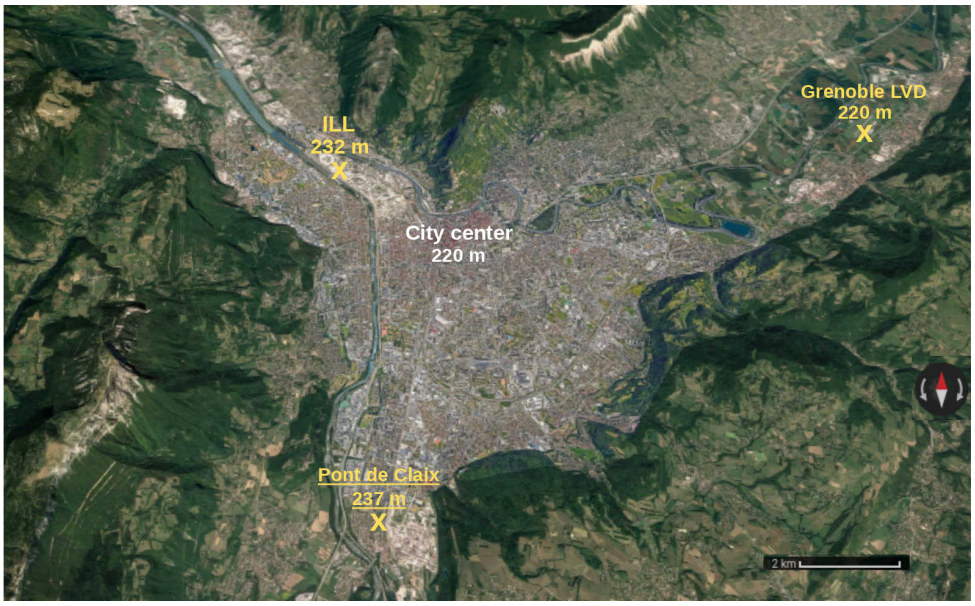

Figure 2.1: Sattelite map of the valley of Grenoble. In yellow, the location and altitude of three stations can be seen: the station at the Institute Laue-Langevin (ILL), at Aérodrome Grenoble Le Versoud (Grenoble LVD) and the Pont de Claix station (underlined). Additionally, the city center is shown in white.

[1] www.atmo-auvergnerhonealpes.fr

For this study we are interested in the temperatures at the bottom of the valley where the population density is highest, namely in the vicinity of the city center. However, measurements at such location do not exist and weather stations close to this location did not perform measurements during a period longer than 30 years. The Pont de Claix station provides the only time series of measurements which allow a climatological study. In order to verify that the measurements at this location are representative of the whole valley they are compared against two other stations: Grenoble-LVD and the ILL. These other stations are also located at the bottom of the valley (figure 2.1). Due to a constraint in access to a larger data set, only a period of seven years between 2011-2017 is used for this comparison.

The Pont de Claix data is in agreement with that of the Grenoble-LVD and the ILL for the period 2011-2017. Indeed, we find a mean absolute error (MAE) of 1.31 °C and 2.08 °C, a root mean square error (RMSE) of 1.82 °C and 2.59 °C and finally a correlation of 0.98 and 0.96 with Grenoble LVD and ILL, respectively. Therefore, the Pont de Claix observations are deemed representative of the valley bottom and will be used as a benchmark for the model output.

2.1.2 Post-processing of in-situ measurements

The raw data set must be processed due to missing values and the presence of outliers. Firstly, the outliers above or below 4 standard deviations from the average for the MJJASO months are removed. In figure A.1 in appendix A, the removed outliers can be seen. Secondly, a 3rd order spline interpolation is applied to fill single missing values. This allows an increase in data points without generating non-physical temperature fluctuations.

As will be discussed in section 2.2, daily maximum (Tmax) and minimum (Tmin) temperatures are needed to define a heat wave. Thus, one needs to compute Tmin and Tmax from hourly observations. In order to do so, days with missing values must be carefully handled. One would find unrealistic values for Tmin and Tmax if the missing values occur in the crucial period of the day where these extremes take place. Therefore, an investigation of the time periods where these temperatures occur is required. We find that Tmin occurs between 2 and 7 a.m. and Tmax between 11 a.m. and 4 p.m. (figure A.2 in appendix A). Therefore, if a day presents missing values within these periods it is fully discarded, whereas if a day presents missing values outside of these periods it is kept. Following this procedure, we extracted time series for Tmin and Tmax from the raw measurements.

For the period 1984-2014, the Tmin and Tmax series show a mean of 12.6°C and of 25.1°C, respectively. The Tmin series shows a lower variability than the Tmax series with standard deviation of 3.9°C and 6.2°C, respectively. Histograms of Tmin and Tmax as well as their respective Gaussian fit and statistical information can be found in figure A.3 in appendix A.

2.1.3 Model output

In this study, the output from the regional climate model MAR[2] (Modèle Atmosphéric Régional) is used. The model data of MAR is the result of simulations run with boundary forcings provided by the reanalysis ERA5 from the European Centre for Medium-Range Weather Forecasts (ECMWF) and by the global climate model MPI Earth System Model (MPI) from the Max-Planck Institute for Meteorology. The reanalysis ERA5 contains a detailed record of the global

[2] www.mar.cnrs.fr

atmosphere, land surface and ocean from 1950 until present (Hersbach et al. 2020). Thus, the most realistic historical simulation that can be obtained with MAR is when it is forced by ERA5 (MAR-ERA5 for short). In order to use MAR to simulate future periods the GCM MPI is used as lateral forcing (referred to as MAR-MPI). MPI is a global coupled atmosphere–land–ocean–sea ice biogeochemistry model (Keeble et al. 2021). To estimate changes in HW characteristics from 1985 to 2100, this study makes use of two types of MAR-MPI simulations: an historical simulation run from 1985 to 2014 and a future simulation from 2014 to 2100. The historical simulation is used as reference to evaluate changes in HW characteristics in the future. Within the future simulation, three 30-year periods are selected: around 2030 (2016-2045), 2050 (2036-2065) and 2070 (2066-2085). The length of these periods is chosen to correspond to the time scale of climate variability given that we are interested in the climatological evolution of heat wave events. The future simulations follow the newly developed shared socio-economic pathways (SSPs), which provide future emissions and land use changes based on scenarios directly relevant to societal concerns regarding climate change impacts, adaptation, and mitigation (Riahi et al. 2017). Overall, the SSPs follow five categories: sustainability (SSP1), middle of the road (SSP2), regional rivalry (SSP3), inequality (SSP4), and fossil-fuelled development (SSP5). Further, each scenario is associated with a radiative forcing pathway which is the radiative forcing at the top of the atmosphere at the end of the century, in W/m^2. In this thesis, two SSPs are considered:

i) the SSP2 scenario assumes a "middle of the road" development with medium challenges in the mitigation and adaptation to climate change (Fricko et al. 2017) associated with a radiative forcing of $4.5\,W/m^2$. This scenario was chosen since it reflects a plausible outcome given current policies (Hausfather et al. 2020).

ii) the SSP5 scenario assumes a development path that is dominated by extensive fossil-fuel use comprising high challenges to mitigation combined with low challenges to adaptation (Riahi et al. 2017). This scenario is associated with a radiative forcing of $8.5\,W/m^2$. This SSP was chosen to quantify the implications of a worst-case climate scenario in HW events.

Table 2.1: The simulations of the MAR model used in this analysis.

Forcing	Scenario	Period	Short Name
ERA5	-	1985-2014	MAR-ERA5
MPI	-	1985-2014	MAR-MPI-HIST
	SSP5	2016-2045	MAR-MPI-530
		2036-2065	MAR-MPI-550
		2066-2085	MAR-MPI-570
	SSP2	2016-2045	MAR-MPI-230
		2036-2065	MAR-MPI-250
		2066-2085	MAR-MPI-270

The MAR model is a RCM that was developed by Hubert Gallée (Gallée et al. 1994) and is particularly suited to simulate the atmospheric dynamics over mountain ranges (Ménégoz et al. 2020). The output of the MAR model applied with a 7-km resolution over the European Alps is used to investigate changes in HW characteristics. In figure 2.3, the valley of Grenoble, as

represented in the MAR model, can be found. The MAR simulations considered in this work are summarized in Table 2.1. The short names presented in this table are built based on their forcing, SSP scenario and 30-year period. For instance, MAR forced by MPI under SSP5 for the period around 2030 is referred to as "MAR-MPI-530". For this project, we look at the daily maximum and minimum temperatures at 2 meters above the ground. The Tmin and Tmax model data used for this project was provided by the Climat-Cryosphère-Hydrosphère team at the Institut des Géosciences de l'Environment[3] (IGE).

2.1.4 Model validation

In order to study the ability of the MAR model to represent the air temperature at the valley bottom a validation of its output has to be conducted. To this extent, the output MAR-ERA5 is compared to the observations at the Pont de Claix station for the period 1985-2014. The valley bottom is represented by six grid points in the MAR domain (see figure 2.3). Temporal series of Tmin and Tmax are associated with each grid point. The PDFs of Tmin and Tmax provided by the model are compared with the PDFs of the observations (figure 2.2). Furthermore, the MAE between model output and observations is computed. The results for each of these points are relatively similar and only the results for the point with lowest MAE and with PDF characteristics close to the PDF of observations, referred to as P_*, are shown.

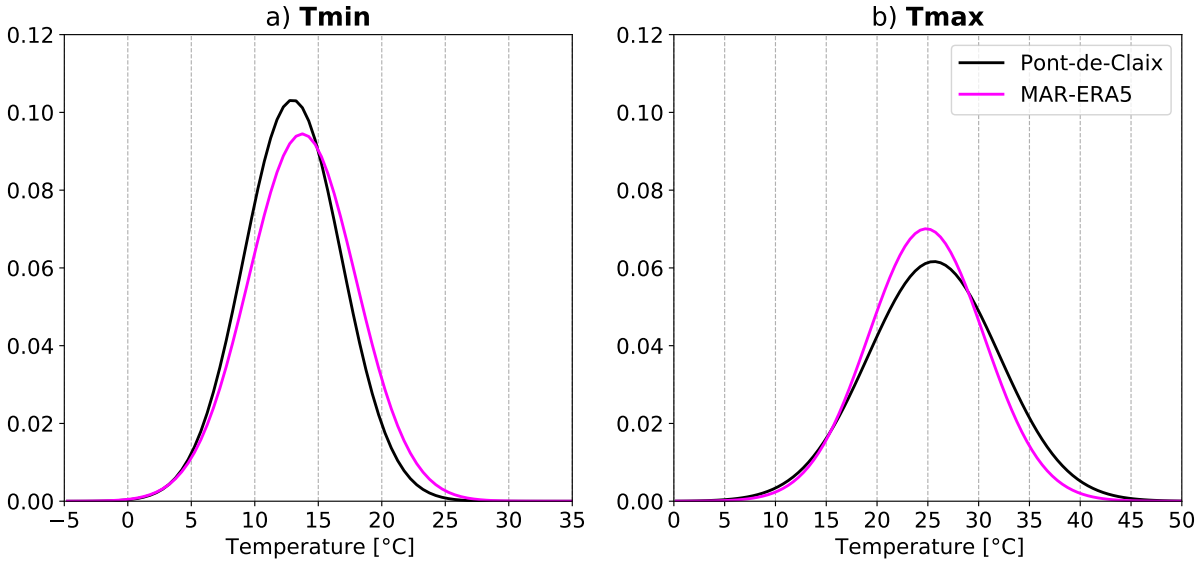

Figure 2.2: Gaussian fits of the histograms of the MAR-ERA5 output (pink) and of the Pont de Claix data (black) for the historical period (1985-2014). On the left, the PDFs for Tmin and on the right, for Tmax.

For P_*, we find a MAE of 2.12°C and 2.41°C for Tmin and Tmax, respectively. The Gaussian fit of the PDFs of Tmin and Tmax for P_* in MAR-ERA5 and of the observations are displayed in figure 2.2. Additionally, the respective histograms and Gaussian fit are shown in figure A.4 in appendix A.

As can be seen in figure 2.2, the MAR-ERA5 model is able to represent the mean Tmin and Tmax temperatures to an accuracy of less than 1°C. Further, the variability of the model is

[3] www.ige-grenoble.fr

representative of the observations with differences in standard deviation of less than 1°C. For Tmin, the model presents a higher variability (figure 2.2a) whereas for Tmax a lower variability is seen (figure 2.2b). Additionally, the left tails of the PDFs for the model match closely to the observations. This indicates that MAR-ERA5 depicts well the lower temperature extremes of both Tmax and Tmin. On the other hand, it can be seen that the right tails of the PDFs do not match: the model is slightly overestimating Tmin and underestimating Tmax. Therefore, this inaccuracy in the higher extremes of the PDF should be accounted for when interpreting the results. The overestimation of MAR-ERA5 for Tmin might be explained by the fact that MAR overestimates temperature at low altitudes (Beaumet et al. 2021). Furthermore, the underestimation of Tmax might be explained by the altitude difference between P_* (422 m) and the measurement station (237 m).

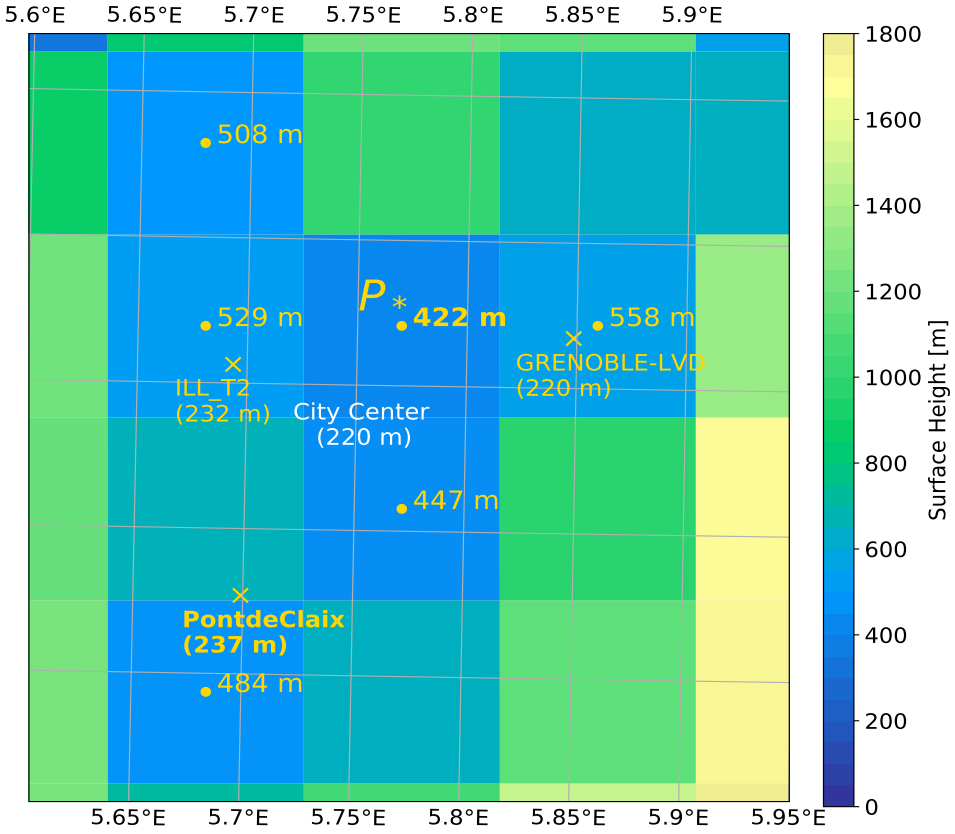

Figure 2.3: MAR model representation of the valley of Grenoble with a resolution of 7 km. In yellow, the location (denoted with a cross) and altitude of three stations can be seen: the station at the Institute Laue-Langevin (ILL_T2), the one at Aérodrome Grenoble Le Versoud (Grenoble LVD) and the Pont de Claix station (bold). Points in yellow, represent the six grid points under study as well as their altitude in MAR. Additionally, the best grid point, P_*, can be found in the center of the image with an altitude of 422 m. Finally, the city center is shown in white.

2.2 Heat wave definition and characteristics

2.2.1 Heat wave definition

A heat wave (HW) is a period of extremely high temperature. A universal definition of a heat wave cannot be made because it depends on the sector of interest which could be human health, electricity supply, transportation, agriculture and so on (Perkins et al. 2013; Perkins 2015). A range of meteorological variables can be used to define a heat wave. In this work, the interest lies on the impacts of these extreme events on human health and mortality. Since the health effects of HWs are mostly severe when there is a lack of relief between hot days (Pezza et al. 2012), the definition of HW must include thresholds for both maximum and minimum temperature. The combination of the minimum and maximum temperature above specific thresholds has been shown to out perform other meteorological indicators by presenting a clear relationship with excess mortality (Pascal et al. 2006). Generally, HWs are defined using either an absolute threshold (a fixed value of temperature) or a relative threshold such as a percentile-based value of temperature. The latter is the most interesting since it relates the definition of HW to the considered time period and location. This is an advantage because it allows for the detection of heatwaves across different locations. For HWs related to human health impacts, the period of at least 3 consecutive days combined with percentile-based thresholds for Tmin and Tmax is widely used in literature (e.g. Perkins et al. 2013; Antics et al. 2013; Cowan et al. 2014; Russo et al. 2015). Hence, for this project, a HW is defined as a *period of at least 3 consecutive days for which both the maximum and minimum temperatures are above or equal to the respective 92nd percentile in the historical MJJASO months*. The choice of this percentile will be explained in section 2.2.3.

2.2.2 Heat wave characteristics

Most of the impacts of temperature extremes on human health relate not only to individual hot days but also to other factors such as heat wave duration and peak temperatures (Fischer et al. 2010). Thus, for an event-based analysis we focus on the following HW characteristics:

- The duration of a heat wave.
- The maximum temperature reached during a heat wave, T_{peak}.
- The mean daily maximum temperature anomaly of a heat wave, $\overline{T_{max}}'$. The specific computation of this anomaly is explained in the last paragraph of this section.

Furthermore, in order to explore the temporal evolution and quantify climatological changes in heatwave characteristics, a similar methodology to Perkins et al. 2013 is adopted. Thus, the focus is on yearly values of heat wave characteristics. Moreover, we include characteristics related to Tmin which was not done in Perkins et al. 2013. The following HW characteristics are studied:

- **HWN** ("Heat Wave Number"): the number of HWs per year.
- **HWdays** ("Heat Wave days"): the number of HW days per year.
- **HWD** ("Heat Wave Duration"): the duration of the longest yearly heat wave.

- **HWMm** and **HWMx** ("Heat Wave Mean"): the mean value of Tmin and Tmax of the hottest yearly heat wave, respectively. For a given year, the hottest heat wave is taken as the heat wave which presents the hottest mean value of Tmax.
- **HWAm** and **HWAx** ("Heat Wave Amplitude"): the maximum Tmin and Tmax of the hottest yearly heat wave, respectively. The hottest heat wave is defined as in the previous point.

The calculations of $\overline{T_{max}}'$, HWAm, HWAx, HWMm and HWMx are anomaly-based. These anomalies are computed by subtracting the 92nd percentile for the historical MJJASO months from the value of the HW characteristic, depicting how much hotter heat wave peaks and means are when compared against the HW defining threshold. All of these characteristics are expected to become more severe, already for the period around the year 2030 and to an increasingly stronger extent by around 2050 and 2070. For this work, using the aforementioned HW definition, each HW characteristic is calculated yearly for the time span 1985-2100 and their time evolution is studied. Additionally, each characteristic is analyzed for the 30-year time periods considered in this work (table 2.1).

2.2.3 Validation of heat wave definition

The percentile threshold must be defined taking into account that one should recover a large enough number of HWs for a statistically relevant analysis. On the other hand, the HWs must remain realistic both in quantity and duration. The 92nd percentile is chosen because it allows to recover a significant population of HW events in the output of MAR-ERA5. We find (not shown) that using a smaller percentile results in too many or too long events whereas using a larger percentile yields too few HWs. This percentile comes as the result of an iterative approach for selecting the optimal threshold by comparing HWs in MAR-ERA5 to real, documented HWs.

The historical 92nd percentiles in MAR-ERA5 are 17.8°C for Tmin and 33.8°C for Tmax. The HWs detected in MAR-ERA5 are shown in figure 2.4 where their maximum temperature, duration and $\overline{T_{max}}'$ are depicted. The HW of August 2003 can be easily found on the right side of the plot given its abnormally long duration. However, its maximum temperature is not captured by the model (during this HW temperatures surpassed 40°C). This is expected since, as seen in section 2.1.4, the MAR model is underestimating the upper tail of maximum daily temperatures. In figure 2.4, one can also easily identify a HW occurring in Grenoble in August 2011. The only matching HW that could be found in documentation was located in Puy-de-Dôme (CIRE Auvergne 2011) reaching a maximum temperature of about 40°C and during 5 days. However, it is not unrealistic to consider that a HW could have also occurred in Grenoble around that time given the synoptic length scale of high-pressure systems that give rise to this type of extreme events (Perkins 2015).

In appendix A, a table with documented HWs in and around Grenoble and their corresponding representation in the MAR-ERA5 output is exhibited (table A.1). This table summarizes the literature review on documented heatwaves and compares them to the events found in MAR-ERA5. The documented locations vary greatly amongst papers (e.g. western Europe as in Schoetter et al. 2015, France as in Fouillet et al. 2007 or Lyon as in Antics et al. 2013) and thus, for some locations this table serves solely as an indication that an extreme event occurred either in the vicinity of Grenoble or in an extended area encompassing Grenoble. Nonetheless, using our definition of HW in the MAR-ERA5 model allows us to identify most of the HWs

documented between 1985 and 2014. More precisely, the HWs in MAR-ERA5 either exactly match the documented period, match the period but differ in duration by 1 to 3 days (both longer or shorter duration), or are shifted by 1 to 2 days.

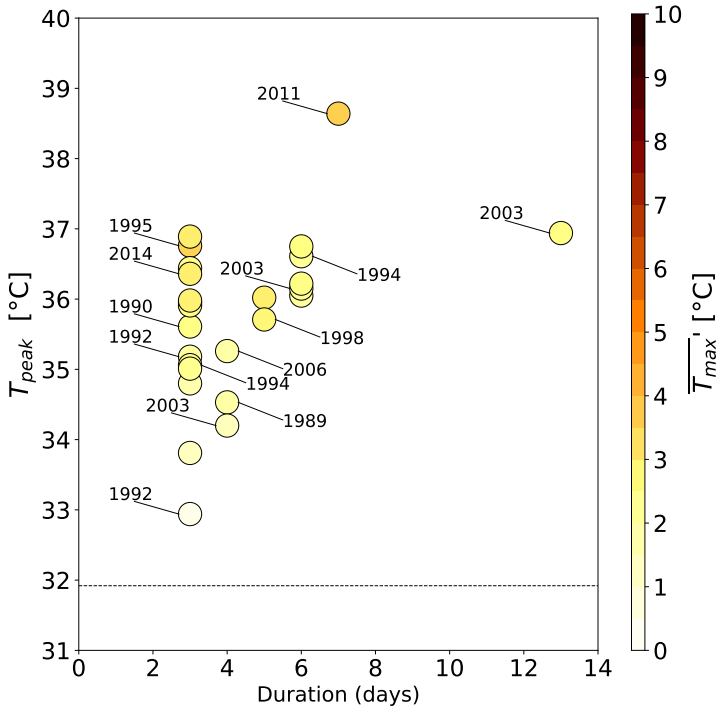

Figure 2.4: Heat waves detected during the 1985–2014 period with MAR-ERA5. Each bubble gives the duration (x axis), peak temperature (y axis) and mean daily temperature anomaly (bubble color). This anomaly is computed with respect to the 92nd percentile calculated for MAR-ERA5 (the threshold is indicated by the horizontal blackline).

Chapter 3

Results and discussion

3.1 Probability density functions of Tmin and Tmax

3.1.1 Historical period

In section 2.1.4, the PDFs for Tmin and Tmax for MAR-ERA5 were found to be similar to the PDFs of the observations and therefore, the temperature output of MAR-ERA5 was deemed representative of the valley bottom's temperature. In this section, the MAR-ERA5 PDFs are compared to the PDFs of MAR-MPI-HIST. This allows the quantification of the biases introduced by the forcing given by the MPI model.

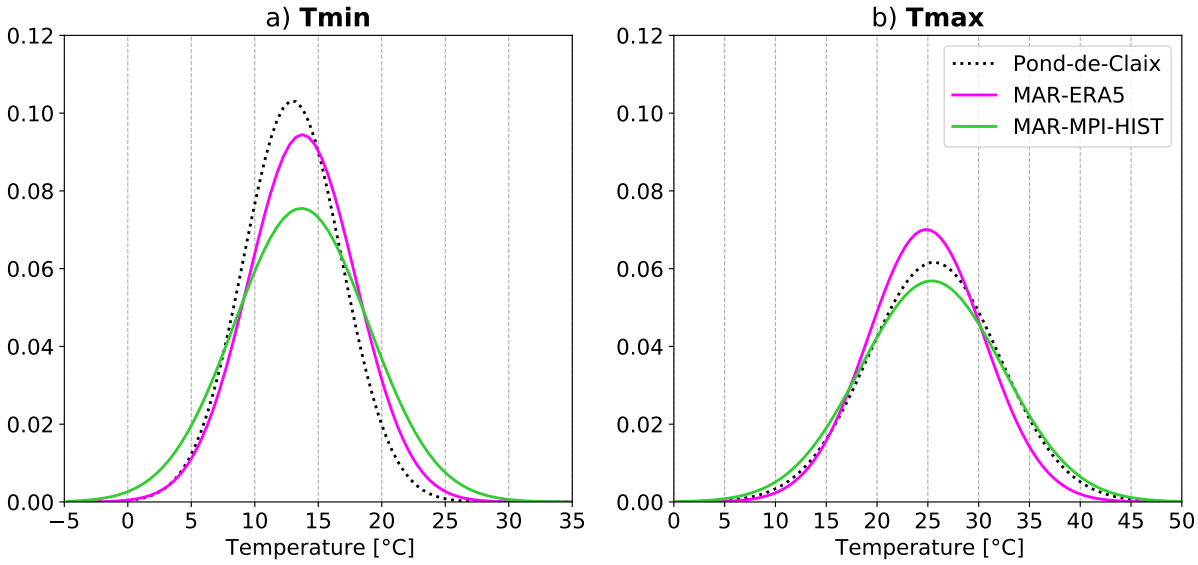

Figure 3.1: Gaussian fits of the histograms of the MAR-ERA5 output (pink), of the MAR-MPI-HIST output (green) and of the Pont de Claix observations (black) for the period 1985-2014. On the left, the PDFs for Tmin and on the right, the PDFs for Tmax.

In figure 3.1, the PDFs for the PodC observations, MAR-ERA5 and MAR-MPI-HIST data are shown. For Tmin (figure 3.1a), the average values for the two MAR simulations are the same, equal to 13.7°C. For Tmax (figure 3.1b), MAR-MPI-HIST has an average value of 25.4°C which is larger by 0.6°C when compared to MAR-ERA5. We observe that the PDFs for MAR-MPI-HIST are closer to the PDFs of the observations than to the PDFs for MAR-ERA5. However, this close match does not mean that the MAR-MPI model will be as representative of the future PDFs as it is for the historical PDF. This similarity between the two curves might be the net product of a bias compensation from the forcing provided by MPI and the MAR model.

The MAR-MPI-HIST shows a higher variability than the MAR-ERA5 for both Tmin and Tmax. This can be easily seen by looking at the standard deviation and the increase in the 92nd percentile. For Tmin, the standard deviation is larger than for MAR-ERA5 by 1.1°C leading to a 1.2°C increase in the 92nd percentile. This increase in percentile value is solely due to the increase in variability since the average value matches for both PDFs. For Tmax, the increase in standard deviation is stronger than for Tmin. This quantity has a standard deviation 1.3°C larger than for the MAR-ERA5 model. This together with the rightward shift of the PDF translates to a 1.9°C increase in the 92nd percentile. Therefore, MAR forced by the MPI model is comparable to MAR-ERA5 in terms of average temperature values but overestimates the probability of temperature extremes.

3.1.2 Future periods

The PDFs of all future 30-year periods (table 2.1) present a shift to the right for both Tmax (figure 3.2) and Tmin (appendix B; figure B.2). This is the case regardless of the SSP scenario. However, the rate at which the rightward shift occurs differs between SSP2 and SSP5. The Tmax output of MAR-MPI for the historical period presents an average value of 25.4°C. By comparison, the average Tmax for the period around 2030 under the SSP2 scenario increases by 1.3°C (figure 3.2a). This increase is 0.4°C higher than in the SSP5 scenario (figure 3.2a) which leads to a stronger shift to the right for the milder scenario. This is clearly illustrated by figure B.1 in appendix B where the full time series of Tmin and Tmax are plotted. It can be seen that the SSP2 scenario yields higher Tmin and Tmax than SSP5 until around 2030. Then, the Tmin and Tmax are similar for both scenarios until around 2050. Hence, the disparity between the PDFs of the two SSP scenarios in the first half of the century can be explained by the fact that Tmax and Tmin only start diverging significantly at around 2050. At first glance, this difference in the two scenarios is not expected since the global temperature in SSP5 is usually higher than in SSP2 from about 2030 as shown in Cook et al. 2020 and Sung et al. 2021. However, these studies consider global means and ensemble means whereas here we consider a single grid point and a single run of a single GCM. Thus, this disparity in the earlier future periods might be possible. Nonetheless, for periods after 2050, the SSP5 scenario predicts a faster increasing trend for both quantities than the SSP2 scenario, with Tmin and Tmax about 2.5°C higher on average for SSP5 than for SSP2, towards the end of the century (figure B.1 in appendix B).

For the 30-year periods around 2050 and 2070 the rightward shift is more prominent for the SSP5 scenario, especially for the latter period. Hence, the PDFs in the SSP2 scenario exhibit a faster shift in the earlier period followed by an increasingly slower shift as it approaches the end of the century. On the contrary, the PDFs of teh SSP5 scenario display a slower shift in the earlier period succeeded by an increasingly faster shift towards the end of the century. The discussion for Tmin is similar and therefore, will be omitted in the text. The PDFs for Tmin for both scenarios can be found in figure B.2 in appendix B.

Throughout all periods, MAR-MPI predicts a nearly constant standard deviation for the SSP2 scenario whereas, for the SSP5 scenario, the most significant increase in standard deviation occurs for the period around 2050 with a value of 0.4°C above the historical reference. The differences in standard deviation for both scenarios with respect to the historical period are much smaller than the differences in the mean values. Further, when looking at the 92nd percentile values we note that these are always about 8°C above the means. Thus, the increase in very hot maximum temperatures in the future is mainly due to the shift of the PDF towards

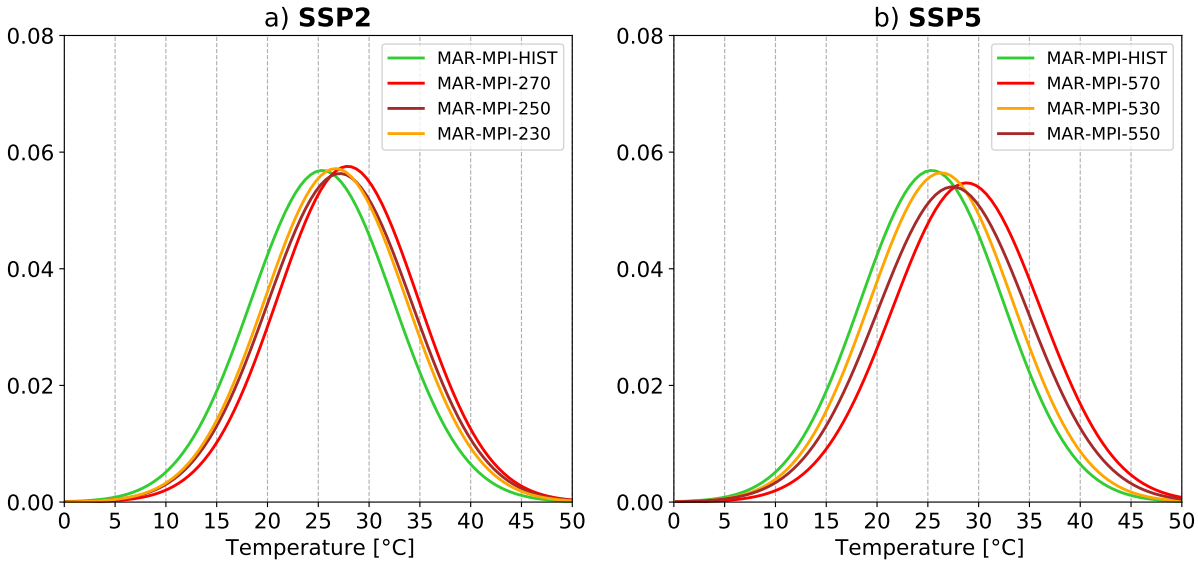

Figure 3.2: Gaussian fits of the histograms of the MAR-MPI-HIST daily **Tmax** output (green) and for the MAR-MPI daily **Tmax** outputs for the future periods around 2030, 2050 and 2070 (yellow, brown and red, respectively). On the left, the PDFs for the SSP2 scenario and on the right, the PDFs for the SSP5 scenario.

higher temperatures, rather than its broadening. Additionally, these changes in the future PDFs of Tmax might lead to an increase in the number and duration of extreme events.

Concluding, the rightward shift of the PDFs is the result of a predicted future increase in mean maximum temperature in Grenoble. For instance, with respect to the historical period, the SSP2 and SSP5 scenarios read, respectively a 2.5°C and 3.4°C increase for around 2070. It is thus expected that the Grenoble valley will suffer an increase in mean daily maximum summer temperatures as well as an increasing probability of extreme temperature events. This conclusion can be generalized to the mean daily minimum summer temperatures for which the discussion is similar (see appendix B; figure B.2).

3.2 Heat wave events in Grenoble

In this section, we analyze the HW events that are found using the MAR-MPI output. We introduce the notation <> to denote the average of a quantity taken over a 30-year period. For the sake of brevity, we use the acronyms found in table 2.1 to refer to the data associated with each model run.

3.2.1 Event-based analysis

The HW events detected in MAR simulations are analysed, considering the HW characteristics described in section 2.2.2. First, we check if HWs in MAR-MPI are statistically comparable to HWs found in MAR-ERA5. For this purpose, we use a bubble plot (figure 3.3a) to depict HWs in the historical period of MAR-MPI. This figure is analogous to figure 2.4 where HW events found in MAR-ERA5 are represented. MAR-MPI-HIST and MAR-ERA5 provide comparable total number of HWs, average duration and $< T_{peak} >$ but HWs in MAR-MPI have a 20.8%

higher $< \overline{T_{max}}' >$ (table 3.1). This increase with respect to MAR-ERA5 seems to be caused by the larger variability intrinsic to MAR-MPI (section 3.1.1).

Table 3.1: Heat wave characteristics averaged per 30-year period. The value within parenthesis is the percentage increase in relation to MAR-MPI-HIST. The mean Tmax anomaly is computed against the 92nd historical percentile threshold for daily maximum temperature (Tmax). This threshold corresponds to 33.8°C for MAR-MPI-HIST and 31.9°C for MAR-ERA5.

	1985-2014			2016-2045	2036-2065	2056-2085
	ERA5	MPI		MPI	MPI	MPI
Total number of HWs [-]	26	28	SSP2	56 (+100%)	77 (+175%)	77 (+175%)
			SSP5	53 (+89%)	94 (+236%)	125 (+346%)
$< T_{peak} >$ [°C]	35.8	38.0	SSP2	38.6 (+1.6%)	38.7 (+1.8%)	38.8 (+2.1%)
			SSP5	38.9 (+2.4%)	38.8 (+2.1%)	39.4 (+3.7%)
Average Duration [days]	4.4	4.5	SSP2	4.5 (+0%)	5.1 (+13.3%)	5.2 (+15.6%)
			SSP5	5.2 (+15.6%)	5.7 (+26.7%)	6.3 (+40%)
$< \overline{T_{max}}' >$ [°C]	2.4	2.9	SSP2	3.0 (+3.4%)	3.0 (+3.4%)	3.1 (+6.8%)
			SSP5	3.1 (+6.8%)	3.1 (+6.8%)	3.4 (+13.6%)

The values for MAR-MPI-HIST in table 3.1 are used to quantify the percentage increase for the future periods. For both SSP scenarios, an increasing trend for all metrics is seen when departing from the historical period towards future periods, especially in the total number of HWs (table 3.1). Around 2030, we find two times more total number of HWs with respect to the period 1985-2014 in both scenarios. For the other two 30-year periods, the two scenarios diverge. For the SSP2 scenario, we find 175% more HWs around 2050 and around 2070. On the other hand, the SSP5 scenario shows a continuous increase with respect to the reference of 236% and 346% more HWs around 2050 and 2070, respectively.

Not only HWs seem to become more frequent, their $< T_{peak} >$ and $< \overline{T_{max}}' >$ as well as their average duration increase as we move towards the end of the century (figure 3.3). For the SSP2 scenario (figures 3.3b, 3.3d, 3.3f), these increments are subtle but present, while for the SSP5 scenario (figures 3.3c, 3.3e, 3.3g), they are more prominent.

For both scenarios in figure 3.3, one can see multiple HW events with T_{peak} well above 40°C, in some occasions HWs can get as hot as 45°C for the future periods. However, as was discussed in section 3.1.1, MAR-MPI overestimates the probability of extreme Tmax. Thus, these absolute values of temperature must be interpreted with care.

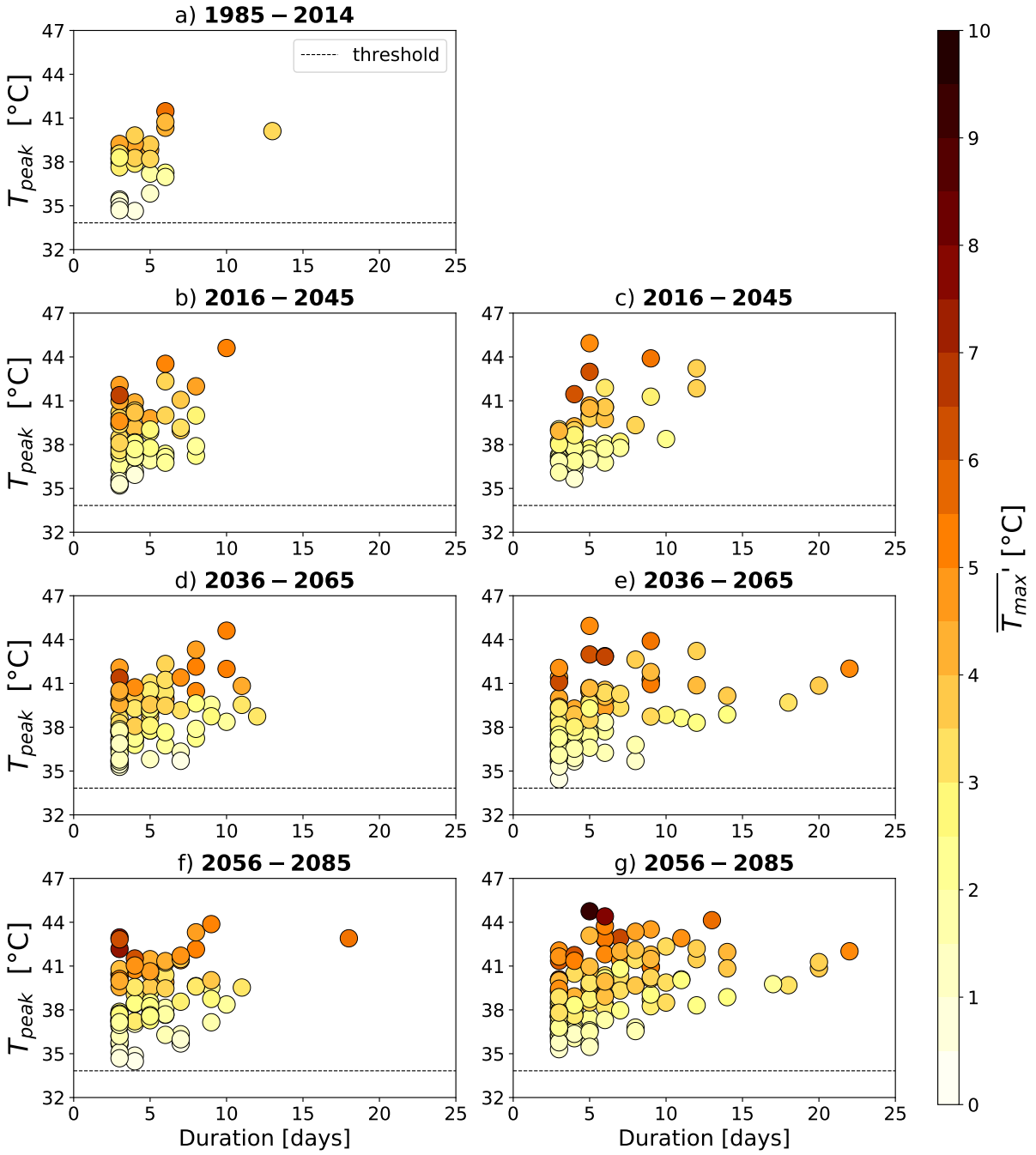

Figure 3.3: Heat wave events detected in MAR-MPI for all 30-year periods. Plot a) shows MAR-MPI-HIST results, plots b), d) and f) belong to the SSP2 scenario and plots c), e) and g) to the SSP5 scenario. Each bubble gives the duration (x-axis), peak temperature (y-axis) and mean daily maximum temperature anomaly (color). This anomaly is computed against the 92nd historical percentile for Tmax in MAR-MPI. This threshold is indicated by the horizontal black line. The number of displayed bubbles corresponds to the total number of heatwaves (table 3.1).

3.2.2 Yearly-based analysis

In this section, the yearly HW characteristics described in section 2.2.2 and their 30-year means are studied. For this purpose, the boxplot for each HW metric is computed in figure B.3 in appendix B. These plots provide information on the spread, interquartile range, median and mean of the characteristics per period. We observe that the HWN, HWD and HWdays found in MAR-MPI-HIST are comparable to the ones found in MAR-ERA5. Thus, these HW metrics might be well represented in MAR-MPI for future periods. On the other hand, the HWA and HWM for both Tmin and Tmax differ between these two simulations: MAR-MPI-HIST shows both a larger mean and wider interquartile range as well as a larger spread. The larger mean values show that in MAR-MPI-HIST the HWA and HWM are further away from the historical 92nd percentile than in MAR-ERA5. Moreover, the larger spread is an indicator of the higher variability in the MAR-MPI model. This in agreement with the discussion in section 3.2.1 where it was found that the HW events in MAR-MPI-HIST had higher $< T_{peak} >$ and $< \overline{T_{max}}' >$ than in MAR-ERA5.

As observed in section 3.2.1, the overall trend across the metrics and SSP scenarios shows an increase in the mean values and in the spread (figure B.3). For SSP2, we find a slower increase in the mean from period to period than for SSP5. For the milder scenario the two last periods show similar mean value and differ slightly in interquartile range and spread. This demonstrates that HW characteristics around 2070 with SSP2 will remain comparable to around 2050 on the mean, but the later period will show higher variability.

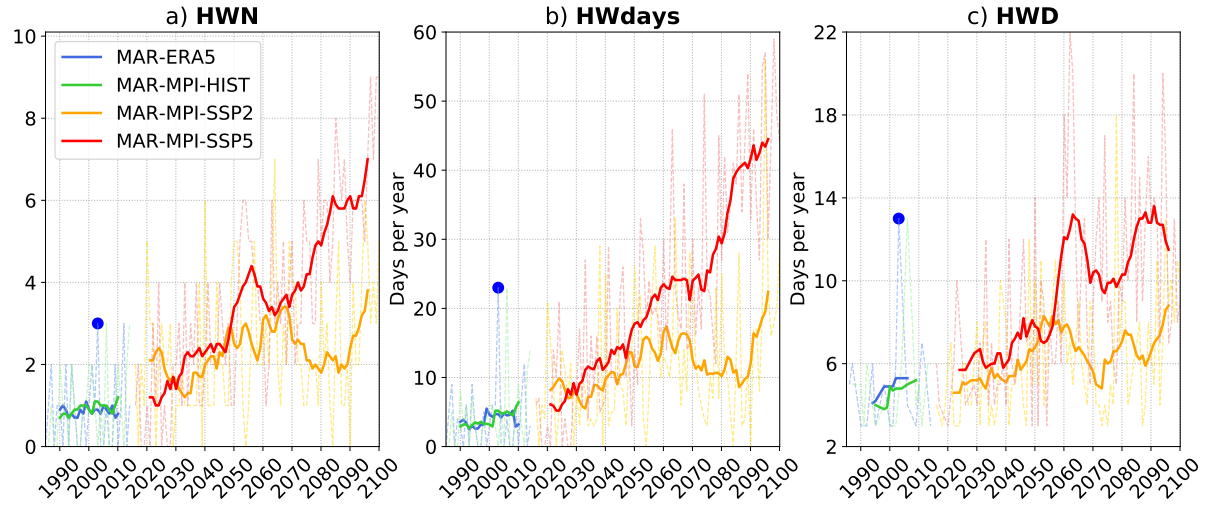

Figure 3.4: Time evolution of a) HWN (yearly number of HWs), b) HWdays (total number of HW days per year) and c) HWD (duration of longest HW per year) for the period 1985-2100. The solid lines are obtained with a 10-year moving average. The blue dot represents the year 2003 obtained with MAR-ERA5.

We now focus on the time evolution of the yearly HW characteristics. Figure 3.4 illustrates the progression over the century of the HWN (figure 3.4a), HWdays (figure 3.4b) and HWD (figure 3.4c) for both SSP scenarios. MAR-MPI-HIST and MAR-ERA5 display similar resultss during the reference period. Furthermore, MAR-MPI for both future scenarios shows an increasing tendency for all metrics, especially for HWN and HWdays.

In accordance with the results of previous sections, the two scenarios are similar for the 2030

period (figure 3.4). In particular, we find that on average both simulate an additional HW per year than in the historical period (HIST: <HWN> = 1), about 6 more HW days per year (HIST: <HWdays> = 4) and with the longest HW per year lasting about 1 day longer than in the reference period (HIST: <HWD> = 5). After the year 2050, the two scenarios start to diverge with a rapid increase in HWN and HWdays for SSP5 and a slower increase of the same quantities for SSP2. In the latter, the increase stops in the last three decades of the century. For HWD, it seems that both scenarios increase during the first half of the century and then display an oscillation-like behaviour for the second half with the SSP2 scenario fluctuating about 6 days and the SSP5 at about 11 days. It seems that, with respect to the historical period, the number of HWs per year and the number of HW days per year in Grenoble doubles around 2030 and increases 4-fold (SSP2) and 6-fold (SSP5) in the second half of the century. However, the duration of the longest yearly event seems to be bounded from the second half of the century.

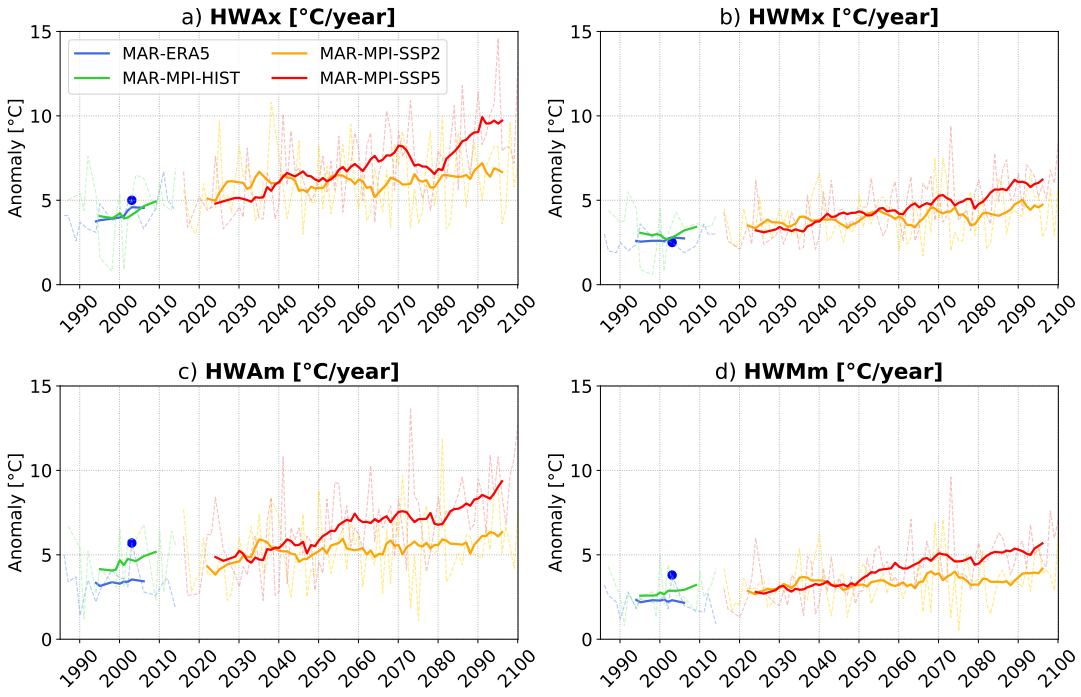

Figure 3.5: Time evolution of a) HWAx and c) HWAm ("Heat Wave Amplitude": the maximum Tmax and Tmin of the hottest yearly event) and of b)HWMx and d) HWMm ("Heat Wave Mean": the mean Tmax and Tmin across the hottest yearly eventy) for the period 1985-2100. The solid lines are obtained with a 10-year moving average.

In figure 3.5, the time evolution of HWA and HWM for Tmax and Tmin can be found. The results of MAR-MPI-HIST are in agreement with MAR-ERA5 for these metrics in the reference period. As the century progresses, HWA and HWM show a slowly increasing trend for both scenarios. At the end of the century, the peak Tmax and Tmin of the hottest HW per year will increase by about 2°C (SSP2) and 5°C (SSP5) with respect to the period around 2000. For the mean Tmax and Tmin of the hottest HW per year the increase is smaller, of about 1°C (SSP2) and 3°C (SSP5).

Overall, climate change seems to impact to a greater extent the amount and duration of HWs than the peak (HWAx and HWAm) and daily mean temperature (HWMx and HWMm) of the

hottest heat waves. However, this conclusion is only valid locally, for Grenoble.

3.2.3 Seasonal distribution of heat wave days

The probability of the occurrence of a heat wave is investigated during the MJJASO months. For this purpose we calculate the probability that a given day is part of a HW event (figure 3.6). For each 30-year period, we take the total number of HW days for a given date. Then, we divide this value by the total number of available dates (which is always equal to 30). For example, the probability of a HW day on the 1st of August, ($P_{01/08}$), is computed as

$$P_{01/08} = \frac{HW_{01/08}}{30} \cdot 100, \tag{3.1}$$

where $HW_{01/08}$ is the number of 1st of August days where a HW was simulated.

For MAR-ERA5, heat waves occur between the 1st of June and the 1st of September. For MAR-MPI-HIST, heat waves are simulated with a lag of about 2 weeks from around the 15th of June to the 15th of September. The highest probabilities of a heat wave day (between 6% and 8%) are simulated for MAR-MPI-HIST between the 20th of July and the 26th of August. This is in agreement with MAR-ERA5 results.

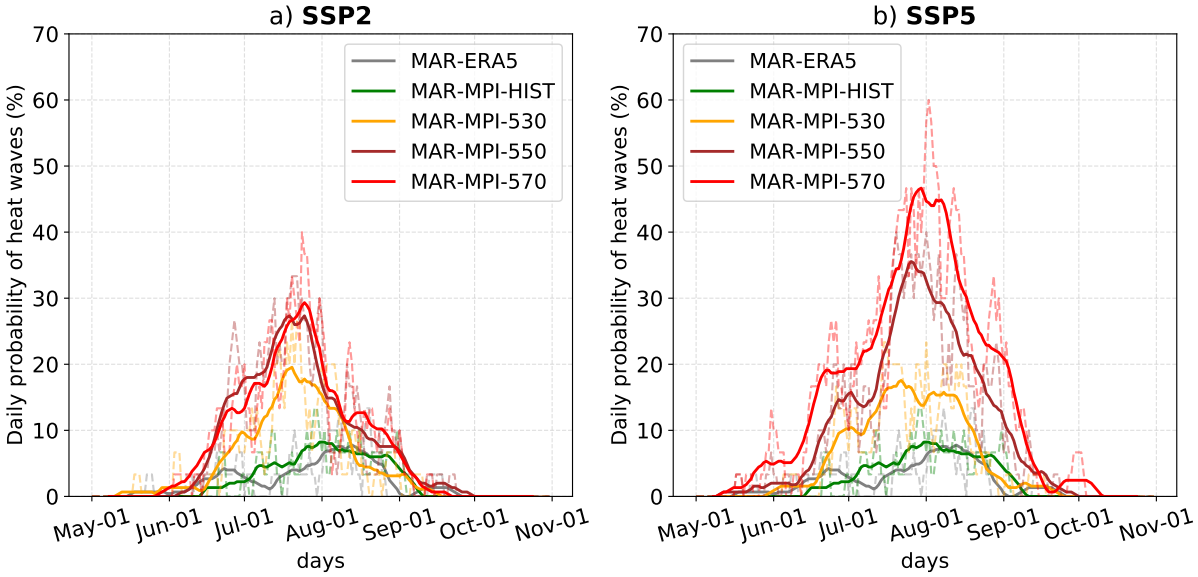

Figure 3.6: Probability of a heatwave day. The full lines are the results of a 15-day moving average.

For the future periods, heat waves occur during a larger part of the summer. For the period around 2030, a probability for a HW day similar or higher than the maximum probability for MAR-MPI-HIST (6-8%) is simulated between the 20th of June and the 15th of August (SSP2) and the 18th of June and the 26th of August (SSP5). For SSP2, the periods around 2050 and 2070 both show similar probability curves. For these periods, a probability of a HW day above the historical probability is found between the 10th of June and the 1st of September. For SSP5, this is seen for dates between the 15th of June and the 10th of September (around 2050) and between the 20th of May and the 15th of September (around 2070). It should therefore be anticipated that HWs might also occur in the months of May and September, especially for the

SSP5 scenario during the second half of the century. The maximum probability of a heat wave day affecting Grenoble is increasing from 6%-8% in MAR-MPI-HIST to about 20% around 2030 for both scenarios. For around 2050, this increase goes up to 28% (SSP2) and 36% (SSP5). At the later part of the century (around 2070) we find the maximum probability increasing to 30% (SSP2) and 46% (SSP5). For all the three future 30-year periods, a heat wave day will become a rather normal situation in July and August.

3.3 Sensitivity analysis to HW defining threshold

In this section, a sensitivity analysis will be performed on the heat wave defining threshold. Two different thresholds will be considered: the 98th historical percentile and the 98th percentile of each 30-year period for Tmin and Tmax. Defining HWs using a very high percentile threshold is common in epidemiological studies (Pascal et al. 2006; Antics et al. 2013). This is due to the fact that excess mortality starts to steeply increase from the 98th temperature percentile (Pascal et al. 2013). Thus, the 98th percentile is more relevant in terms of prediction of HWs with adverse health effects than the 92nd percentile. As will be seen in this section, this choice of percentile drastically lowers the population of HWs simulated with the MAR model. Hence, a statistical analysis of HWs using such percentile would not be informative. The study presented in this section is a sensitivity analysis that provides further insights on the role of the threshold choice.

3.3.1 Definition of HW based on the historical 98th percentile

A total of 3 HWs are detected in MAR-ERA5 (figure 3.7) using the 98th percentile as a threshold. All of these HWs have a duration of 3 days which corresponds to the minimum requirement of our definition. Two of them were found in literature (see table A.1 in appendix A): the 2003 heat wave between the 11th-13th of August and a HW in 2012 between the 19th-21st of August. Hence, using such a threshold to find HWs in MAR-ERA5 does not seem to be effective for a statistically relevant analysis.

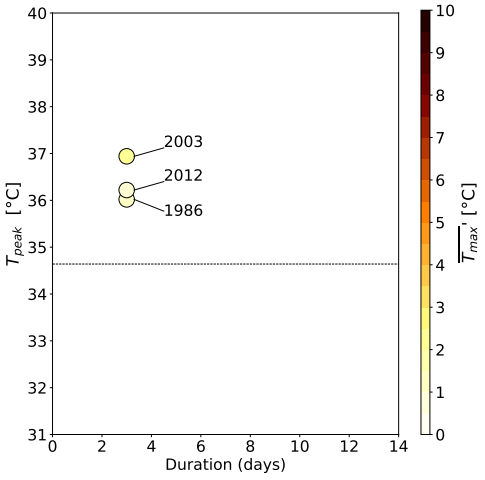

Figure 3.7: Same as in figure 2.4 but using the 98th percentile of Tmax and Tmin in MAR-ERA5 to define a heat wave event. This threshold is indicated by the horizontal blackline.

In figure 3.8a, a bubble plot similar to the one in figure 3.3a is displayed for MAR-MPI-HIST. This figure is complemented by table 3.2. HWs in MAR-MPI-HIST are comparable with MAR-ERA5 in amount and duration but they present higher temperatures. In MAR-MPI-HIST, a total of 5 HWs are found with an average duration of 3.2 days, a $< T_{peak} >$ of 39.9°C and a $\overline{T_{max}}'$ of 2.9°C. This shows that this definition of HWs, when compared to the definition introduced in section 2.2, yields less HWs. Additionally, these HWs are shorter and have higher average peak temperature, $< T_{peak} >$.

Table 3.2: Same as in table 3.1 but using the 98th percentile of Tmax and Tmin in MAR-MPI-HIST to define a heat wave event in MAR-MPI.

	1985-2014			2016-2045	2036-2065	2056-2085
	ERA5	MPI		MPI	MPI	MPI
Total number of HWs [-]	3	5	SSP2	9 (+80%)	9 (+80%)	16 (+220%)
			SSP5	15 (+200%)	26 (+420%)	58 (+1060%)
$< T_{peak} >$ [°C]	36.4	39.9	SSP2	40.7 (+2%)	41.5 (+4%)	41.3 (+3.5%)
			SSP5	40.5 (+1.5%)	40.7 (+2%)	40.9 (+2.5%)
Average Duration [days]	3	3.2	SSP2	3.4 (+6.2%)	4.3 (+34.4%)	4.2 (+31.3%)
			SSP5	3.3 (+3.1%)	4.2 (+31.3%)	4.3 (+34.4%)
$< \overline{T_{max}}' >$ [°C]	1.4	2.2	SSP2	2.8 (+27.3%)	3.3 (+50%)	3.0 (+36.4%)
			SSP5	2.7 (+22.7%)	2.7 (+22.7%)	2.7 (+22.7%)

For this HW definition, the discussion of the HW characteristics and their change from the historical to future periods differs from the definition using the 92nd percentile. For SSP2, an increasing trend for the periods around 2030 and 2050 followed by a decrease around 2070 is seen for all characteristics, except for total number of HWs and their duration. On average, these HWs will become warmer and longer towards the mid-century. Then, towards the end of the century, their $< T_{peak} >$ and $< \overline{T_{max}}' >$ seem to slightly decrease whereas their duration remains similar and their frequency increases (figure 3.8). For SSP5, all metrics seem to increase as the century evolves, especially the amount of HWs which increases by 1060% by the end of the century, with respect to the historical period. However, the bubbles in figure 3.8 for this scenario increase at around the same duration, indicating that the duration of HWs will remain identical. Furthermore, the increase in $< T_{peak} >$ and $< \overline{T_{max}}' >$ also remains similar throughout the periods. Hence, this type of HW seems to increase in quantity as the century evolves but remain similar in terms of $< T_{peak} >$ and $< \overline{T_{max}}' >$.

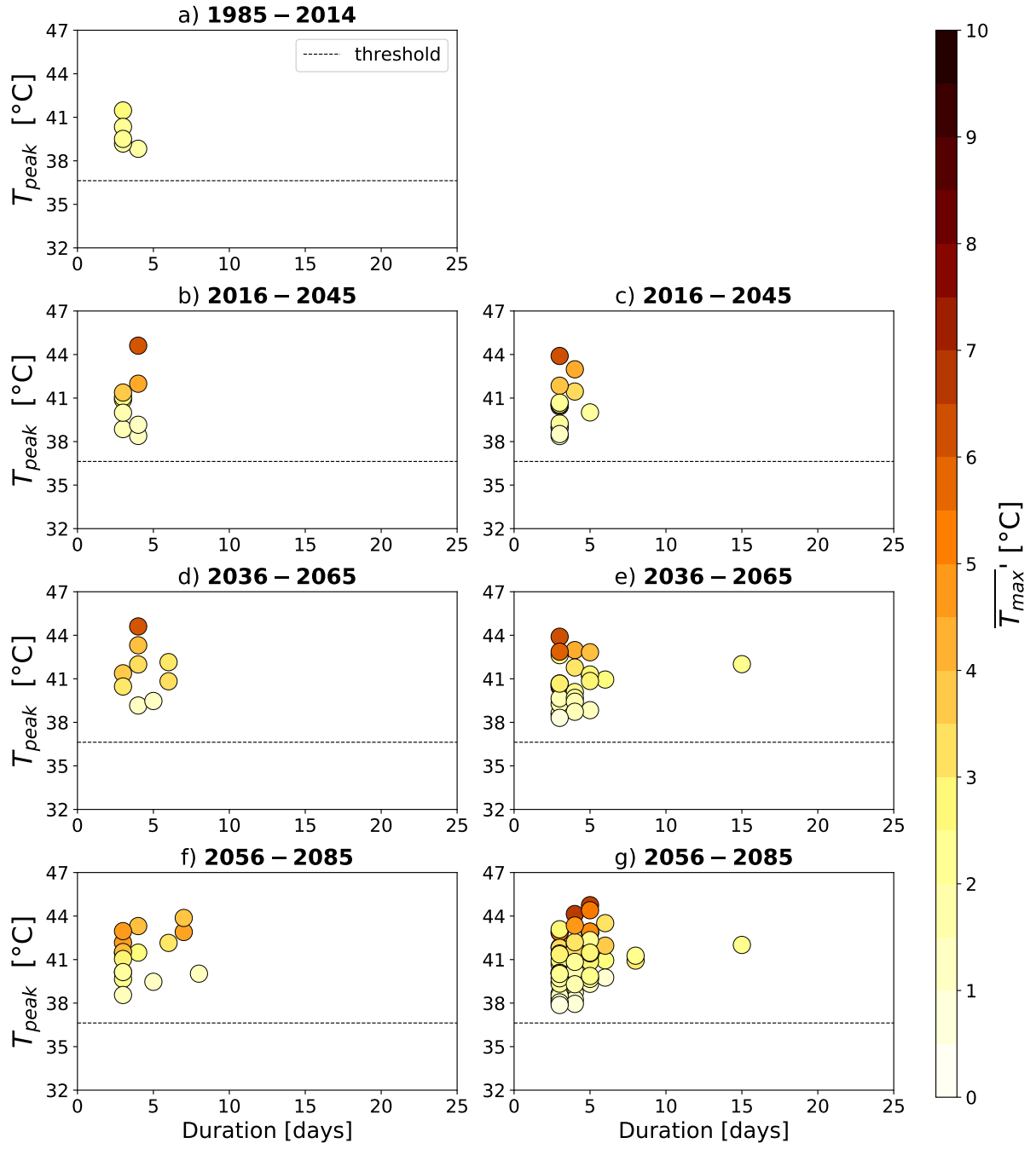

Figure 3.8: Same as figure 3.3 but using the 98th percentile of Tmax and Tmin in MAR-MPI-HIST to define a heat wave event. This threshold is indicated by the horizontal black line.

3.3.2 Definition of HW using the 98th percentile for each 30-year period

Another HW defining threshold that is of interest is the 98th percentile of the same 30-year period where HWs are being searched for. Instead of using the historical climate as a benchmark, this percentile threshold varies in accordance to the considered 30-year period. This is an interesting

study if one assumes that society will find solutions to mitigate the impact of HWs on human health. This definition of HW will correspond to events that are the most extreme, even for the warmer climate of the future.

In figure 3.9, a bubbles plot similar to the one in figure 3.3 can be found. This figure is complemented by table 3.3 where the total amount of HWs per period as well as the average T_{peak} and average mean Tmax anomaly are detailed. However, given the small amount of detected HWs, the values in this table must be interpreted with caution.

Table 3.3: Same as in table 3.1 but using the 98th percentile of Tmax and Tmin for the corresponding period.

	1985-2014			2016-2045	2036-2065	2056-2085
	ERA5	MPI		MPI	MPI	MPI
Total number of HWs [-]	3	5	SSP2	2 (-60%)	4 (-20%)	4 (-20%)
			SSP5	3 (-40%)	6 (+20%)	4 (-20%)
$< T_{peak} >$ [°C]	36.4	39.9	SSP2	43.0 (+7.8%)	42.5 (+6.5%)	43.1 (+8.0%)
			SSP5	41.8 (+4.8%)	41.7 (+4.5%)	43.5 (+9.0%)
Average Duration [days]	3	3.2	SSP2	3.0 (-6.3%)	3.2 (+0%)	3.8 (+18.7%)
			SSP5	3.0 (-6.3%)	3.3 (+3.1%)	3.2 (+0%)
$< \overline{T_{max}}' >$ [°C]	1.4	2.2	SSP2	3.9 (+77%)	2.7 (+22.7%)	2.5 (+13.6%)
			SSP5	3.1 (+40.9%)	1.9 (-13.6%)	2.4 (+9.1%)

As seen in the previous section, the choice of the 98th percentile drastically lowers the population of HWs found in the MAR model. For this HW definition, a few, very hot heat waves are detected for each period. With respect to the historical period, the HWs become shorter but with higher peak temperature. The $< \overline{T_{max}}' >$ also increases despite the increasing threshold. The main difference between the two scenarios is the higher and faster increasing threshold shown by SSP5. However, the effect on T_{peak} and $\overline{T_{max}}'$ is small. The duration and peak temperature of these HWs seem to remain similar as the century evolves for both SSPs but also across the periods.

Choice of dates for local HW simulations in Grenoble

The dates corresponding to the heat waves found using the 98th percentile for each period serve as an indicator of a time period for which a very extreme event was simulated by MAR. These dates are used to identify the HWs to be modelled numerically for a posterior work. Such work will entail simulating these HWs at high resolution over the city of Grenoble. For this purpose, another model will be used with MAR-MPI as boundary forcing. The dates in table C.1 (appendix C) correspond to the HWs defined using the 92nd percentile of that period which comprise the dates of the hotter HWs defined in this section.

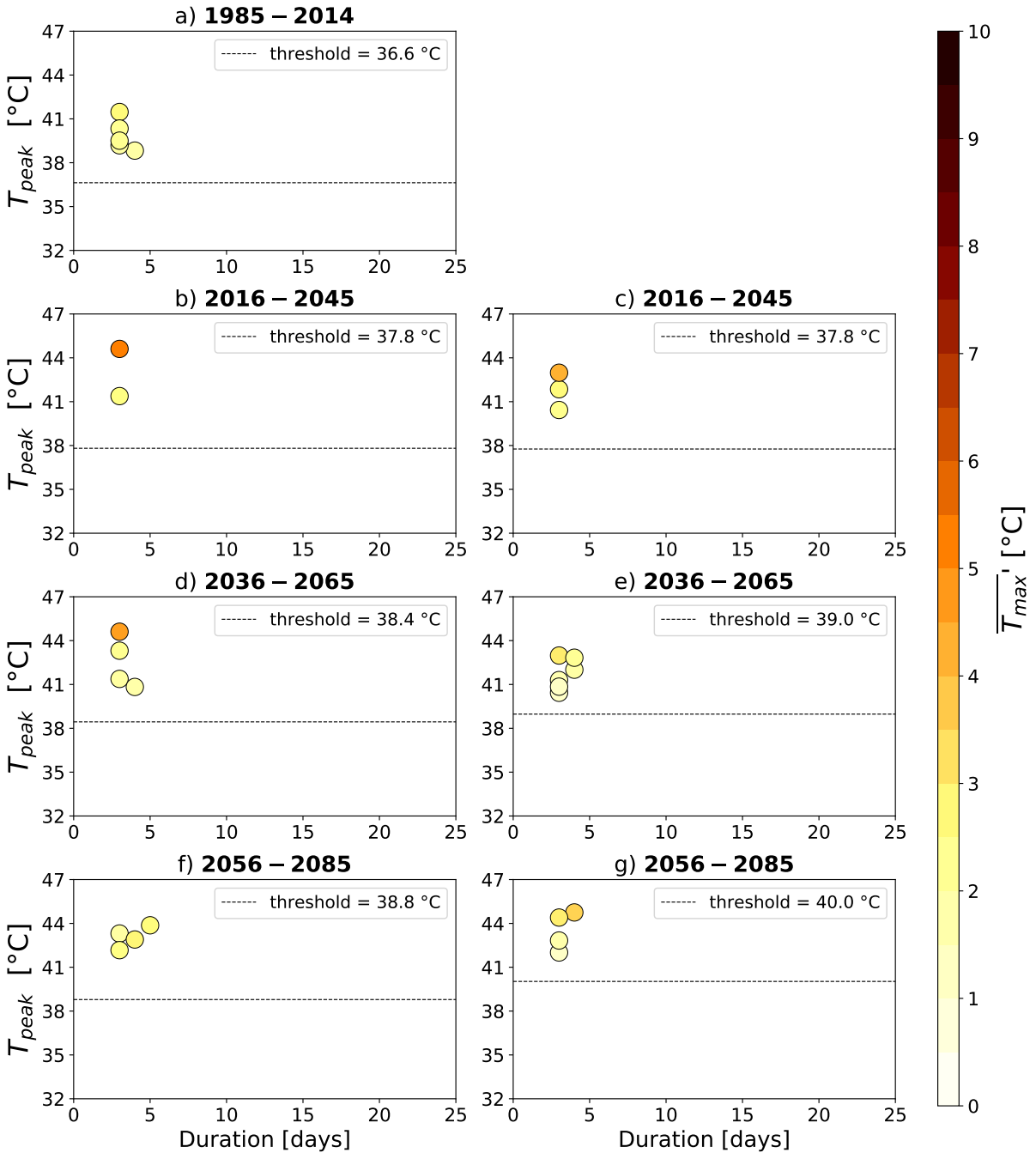

Figure 3.9: Same as figure 3.3 but using the 98th percentile of Tmax and Tmin for the corresponding period to define a heat wave event. This threshold is indicated by the horizontal black line. For a given period, the mean daily Tmax anomaly is computed as the difference to the corresponding threshold.

Chapter 4

Conclusions and outlook

This study provides a comprehensive characterisation of future summer heat waves in the valley of Grenoble under two alternative socio-economic pathways. These were the SSP2 scenario, a plausible scenario given the trajectory of today's society, and the SSP5 scenario, a worst-case premise. A climatological study was achieved using the regional climate model MAR with boundary forcings provided by the reanalysis ERA5 (MAR-ERA5) and by the global climate model MPI (MAR-MPI). We focused on heat waves defined with relation to health impacts given that heat waves can cause a significant impact on population health, including a rise in mortality.

The first part of this work was to validate the capability of the MAR model to reproduce the temperature over Grenoble. Indeed, it was found that MAR-ERA5 is able to represent the mean value and variability of Tmin and Tmax for the historical period (1985-2014). However, for the warmer extremes MAR-ERA5 shows a small overestimation for Tmin and an underestimation for Tmax with respect to the observations. The projections were made using MAR-MPI. This model was compared to MAR-ERA5 during the same past period and we found that MAR-MPI matches the climatological average of Tmin and overestimates the one for Tmax, albeit not significantly. MAR-MPI however, overestimates the climatological standard deviation, indicating a simulated climate which is more variable.

MAR-MPI was considered for three 30-year periods around 2030, 2050 and 2070. The PDFs of Tmin and Tmax shift towards the right due to an increase in mean temperature with respect to the historical period. However, the variability remains similar for all periods. Hence, the increase in very hot daily maximum and minimum temperatures in the future is mainly due to the shift rather than the broadening of the PDF. It was found that the SSP2 scenario exhibits a faster shift in the 2030 period followed by an increasingly slower shift as it approaches the end of the century. On the contrary, the SSP5 scenario displays a slower shift in the 2030 period succeeded by an increasingly faster shift towards the later periods.

Heat waves were defined as periods of at least 3 consecutive days for which Tmax and Tmin are above the 92nd historical percentile. Based on this definition, MAR-ERA5 simulates HW periods which either exactly match documented HWs, match the period but differ in duration by 1 to 3 days or are shifted by 1 to 2 days. Additionally, the MAR-MPI simulates HW characteristics for the historical period in agreement with MAR-ERA5.

It was found that HW events become longer and more common in future periods. They also show increasing trends in their peak and mean daily maximum temperature with respect to the historical period (see table 3.1). Both scenarios simulate twice as many HWs for 2030, about 3 times more in 2050 and 3 (SSP2) and 4 (SSP5) times more for 2070. Additionally, we compute statistics for yearly quantities considering each 30-year period. We find that the yearly HW characteristics present an increase in the mean value and in the spread across SSP scenarios. For SSP2, we find a slower increase in the mean from period to period than in the SSP5.

Furthermore, it was shown that for SSP2 HW characteristics around 2070 remain comparable to around 2050 on average, but the latter period shows higher variability.

The daily probability of the occurrence of a heat wave has also been investigated. For this purpose we calculated the probability that a given day is part of a HW event during the MJJASO months. The probability of a HW day in the future was found to be higher than in the historical period during longer time intervals throughout summer. From 2050 onwards, HW days are 20% more likely to happen from June to September for SSP2, and 30% more likely for SSP5.

A sensitivity analysis to the HW defining threshold has been carried out. This is due to the fact that excess mortality starts to steeply increase from the 98th temperature percentile. Many less HWs are detected using this percentile threshold. For both SSPs, these HWs will become warmer and longer towards the mid-century. Then, towards the end of the century, their duration remains similar and their frequency increases for SSP2. For SSP5 however, HWs keep increasing in duration and temperature until the end of the century. Additionally, the 98th percentile of each 30-year period was used to define HWs. This definition of HW corresponds to events that are the most extreme, even for the warmer climate of the future. With respect to the historical period, the HWs become shorter but with higher maximum temperature. For this definition, the main difference between the two scenarios is the higher and faster increasing threshold shown by SSP5.

For future studies, it would be interesting to quantify the temperature bias of MAR-MPI. Additionally, in order to obtain a more statistically significant study an ensemble of GCMs could be used to force MAR. Then, the HW characteristics could be studied for all runs. Further, if HWs were to be studied from a climate science perspective, the whole domain over the Alps could be taken into account. This would then provide a different study on temperature extremes in high mountain areas and their effect on the melting of glaciers, for example.

Acknowledgements

I would like to express my appreciation to all those who provided their time and effort to help the completion of this master thesis. A special gratitude I give to the project supervisor, Professor Chantal Staquet, for her insightful guidance and feedback throughout the project. I would also like to acknowledge with my deepest appreciation the crucial role of Dr. Sara Bacer, who provided me with wise ideas and strong support during all stages of this project. Additionally, I would like to thank our colleagues from the IGE namely, Julien Beaumet, Martin Ménégoz and Hubert Gallée for carrying out the MAR simulations and providing us with its data.

Bibliography

Antics, Annamaria et al. (Jan. 2013). "A simple indicator to rapidly assess the short-term impact of heat waves on mortality within the French heat warning system". In: *Int. J. Biometeorol.* 57.1, pp. 75–81. ISSN: 1432-1254. DOI: 10.1007/s00484-012-0535-9.

Beaumet, Julien et al. (2021). "Twentieth century temperature and snow cover changes in the French Alps using a high-resolution regional climate model and reanalyses (In review)". In: *Regional Environmental Change*.

Boer, G. J. et al. (Jan. 2001). "Second-order space-time climate difference statistics". In: *Clim. Dyn.* 17.2, pp. 213–218. ISSN: 0930-7575. DOI: 10.1007/PL00013735.

Chaxel, Eric et al. (Jan. 2004). "Production of ozone in the Chamonix Valley (France)". In: *Int. J. Environ. Pollut.* 24, pp. 201–217. ISSN: 0957-4352. DOI: 10.1504/IJEP.2005.007394.

CIRE Auvergne, ARS Auvergne (Nov. 2011). "Bilan des vagues de chaleur des deuxièmes quinzaines de juin et d'août 2011, dans les départements de l'Allier et du Puy-de-Dôme". In: *Bulletin de veille sanitaire* 8, pp. 3–5. URL: https://www.santepubliquefrance.fr/content/download/50907/1099707.

Cook, B. I. et al. (June 2020). "Twenty-First Century Drought Projections in the CMIP6 Forcing Scenarios". In: *Earth's Future* 8.6, e2019EF001461. ISSN: 2328-4277. DOI: 10.1029/2019EF001461.

Coumou, Dim et al. (Sept. 2013). "Historic and future increase in the global land area affected by monthly heat extremes". In: *Environ. Res. Lett.* 8.3, p. 034018. ISSN: 1748-9326. DOI: 10.1088/1748-9326/8/3/034018.

Cowan, Tim et al. (Aug. 2014). "More Frequent, Longer, and Hotter Heat Waves for Australia in the Twenty-First Century". In: *J. Clim.* 27.15, pp. 5851–5871. ISSN: 0894-8755. DOI: 10.1175/JCLI-D-14-00092.1.

D'Ippoliti, Daniela et al. (July 2010). "The impact of heat waves on mortality in 9 European cities: results from the EuroHEAT project". In: *Environ. Health* 9, p. 37. ISSN: 1476-069X. DOI: 10.1186/1476-069X-9-37. eprint: 20637065.

Easterling, David R. et al. (Sept. 2000). "Climate Extremes: Observations, Modeling, and Impacts". In: *Science* 289.5487, pp. 2068–2074. ISSN: 0036-8075. DOI: 10.1126/science.289.5487.2068.

Fischer, E. M. et al. (June 2010). "Consistent geographical patterns of changes in high-impact European heatwaves". In: *Nat. Geosci.* 3, pp. 398–403. ISSN: 1752-0908. DOI: 10.1038/ngeo866.

Fouillet, Anne et al. (July 2007). "Comparaison de la surmortalité observée en juillet 2006 à celle estimée à partir des étés 1975-2003, France". In: *Bulletin épidémiologique hebdomadaire* 22–23, pp. 192–194. URL: http://beh.santepubliquefrance.fr/beh/2007/22_23/beh_22_23_2007.pdf.

Fricko, Oliver et al. (Jan. 2017). "The marker quantification of the Shared Socioeconomic Pathway 2: A middle-of-the-road scenario for the 21st century". In: *Global Environ. Change* 42, pp. 251–267. ISSN: 0959-3780. DOI: 10.1016/j.gloenvcha.2016.06.004.

Gallée, Hubert et al. (Apr. 1994). "Development of a Three-Dimensional Meso-γ Primitive Equation Model: Katabatic Winds Simulation in the Area of Terra Nova Bay, Antarctica". In: *Mon. Weather Rev.* 122.4, pp. 671–685. ISSN: 1520-0493. DOI: 10.1175/1520-0493(1994)122<0671:DOATDM>2.0.CO;2.

Hartmann, Dennis L. et al. (Jan. 2013). "Observations: Atmosphere and surface". In: *Climate Change 2013 the Physical Science Basis: Working Group I Contribution to the Fifth Assessment Report of the Intergovernmental Panel on Climate Change*. Cambridge, England, UK: Cambridge University Press, pp. 159–254. DOI: 10.1017/CBO9781107415324.008.

Hausfather, Zeke et al. (Jan. 2020). "Emissions – the 'business as usual' story is misleading". In: *Nature* 577, pp. 618–620. DOI: 10.1038/d41586-020-00177-3.

Hersbach, Hans et al. (July 2020). "The ERA5 global reanalysis". In: *Q. J. R. Meteorolog. Soc.* 146.730, pp. 1999–2049. ISSN: 1477-870X. DOI: 10.1002/qj.3803.

Keeble, James et al. (Mar. 2021). "Evaluating stratospheric ozone and water vapour changes in CMIP6 models from 1850 to 2100". In: *Atmos. Chem. Phys.* 21.6, pp. 5015–5061. ISSN: 1680-7316. DOI: 10.5194/acp-21-5015-2021.

Mearns, Linda O. et al. (Dec. 1984). "Extreme High-Temperature Events: Changes in their probabilities with Changes in Mean Temperature". In: *Journal of Applied Meteorology and Climatology* 23.12, pp. 1601–1613. DOI: 10.1175/1520-0450(1984)023<1601:EHTECI>2.0.CO;2.

Ménégoz, Martin et al. (Nov. 2020). "Contrasting seasonal changes in total and intense precipitation in the European Alps from 1903 to 2010". In: *Hydrol. Earth Syst. Sci.* 24.11, pp. 5355–5377. ISSN: 1027-5606. DOI: 10.5194/hess-24-5355-2020.

Pascal, Mathilde et al. (Jan. 2013). "Definition of temperature thresholds: the example of the French heat wave warning system". In: *Int. J. Biometeorol.* 57.1, pp. 21–29. ISSN: 1432-1254. DOI: 10.1007/s00484-012-0530-1. eprint: 22361805.

Pascal, Mathilde et al. (Jan. 2006). "France's heat health watch warning system". In: *Int. J. Biometeorol.* 50.3, pp. 144–153. ISSN: 1432-1254. DOI: 10.1007/s00484-005-0003-x.

Perkins et al. (July 2013). "On the Measurement of Heat Waves". In: *J. Clim.* 26.13, pp. 4500–4517. ISSN: 0894-8755. DOI: 10.1175/JCLI-D-12-00383.1.

Perkins (Oct. 2015). "A review on the scientific understanding of heatwaves—Their measurement, driving mechanisms, and changes at the global scale". In: *Atmos. Res.* 164-165, pp. 242–267. ISSN: 0169-8095. DOI: 10.1016/j.atmosres.2015.05.014.

Pezza, Alexandre Bernardes et al. (Jan. 2012). "Severe heat waves in Southern Australia: Synoptic climatology and large scale connections". In: *Clim. Dyn.* 38.1-2, pp. 209–224. ISSN: 0930-7575. DOI: 10.1007/s00382-011-1016-2.

Riahi, Keywan et al. (Jan. 2017). "The Shared Socioeconomic Pathways and their energy, land use, and greenhouse gas emissions implications: An overview". In: *Global Environ. Change* 42, pp. 153–168. ISSN: 0959-3780. DOI: 10.1016/j.gloenvcha.2016.05.009.

Russo, Simone et al. (Nov. 2015). "Top ten European heatwaves since 1950 and their occurrence in the coming decades". In: *Environ. Res. Lett.* 10.12, p. 124003. ISSN: 1748-9326. DOI: 10.1088/1748-9326/10/12/124003.

Schoetter, Robert et al. (Sept. 2015). "Changes of western European heat wave characteristics projected by the CMIP5 ensemble". In: *Clim. Dyn.* 45.5, pp. 1601–1616. ISSN: 1432-0894. DOI: 10.1007/s00382-014-2434-8.

Sung, Hyun Min et al. (Jan. 2021). "Climate Change Projection in the Twenty-First Century Simulated by NIMS-KMA CMIP6 Model Based on New GHGs Concentration Pathways". In: *Asia-Pac. J. Atmos. Sci.*, pp. 1–12. ISSN: 1976-7951. DOI: 10.1007/s13143-021-00225-6.

Ung, Aymeric et al. (Apr. 2013). "Premières estimations de l'impact des vagues de chaleur de 2010, 2011 et 2012 sur la mortalité en France métropolitaine". In: *Bulletin épidémiologique hebdomadaire* 11, pp. 99–103. URL: https://www.santepubliquefrance.fr/determinants-de-sante/climat/fortes-chaleurs-canicule/documents/article/premieres-estimations-de-l-impact-des-vagues-de-chaleur-de-2010-2011-et-2012-sur-la-mortalite-en-france-metropolitaine.

Appendix A

Data

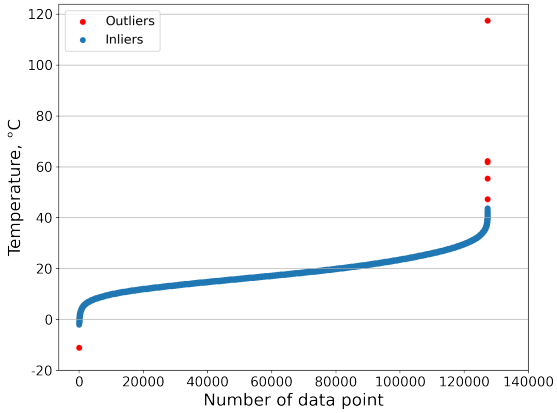

Figure A.1: Observations from the Pont de Claix weather station sorted by temperature value. The horizontal axis is the data point index in the sorted sequence and the vertical axis is the temperature in degrees Celsius. Data points in red are the outliers that were removed from the data set.

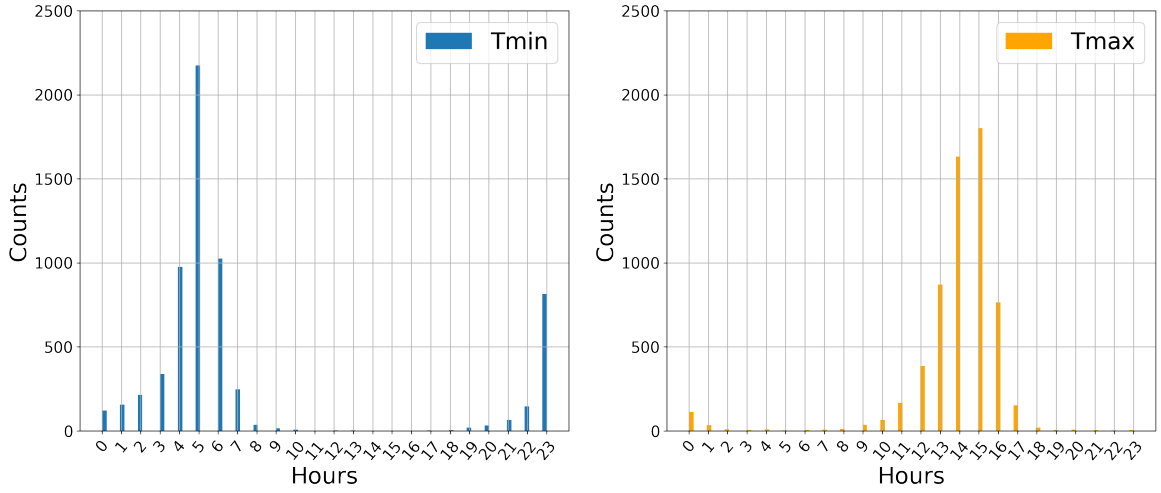

Figure A.2: Counts per hour of daily minimum and maximum temperatures in the observations from the Pont de Claix station. Tmin occurs in the early morning before sunrise and Tmax around 3 hours after midday. For Tmin, a peak is seen at 23h which is an artifact of missing values in the dataset (not shown).

Table A.1: Information about documented heat waves close to Grenoble and of heat waves found in the MAR-ERA5 simulation for the grid point (P_*) above Grenoble.

Reference	**Location**			**Real**	**MAR-ERA5**
		Year	**Month**	**Days**	**Days**
		1986	6	-	26-30
		1987	8	-	14-16
		1987	9	-	13-18
Antics et al. 2013	Lyon	1989	7	21-26	21-24
Schoetter et al. 2015	Western Europe	1990	8	2-4	3-5
		1992	7	-	27-29
Schoetter et al. 2015	Western Europe	1992	8	7-9	6-8
		1994	7	-	2-4
Schoetter et al. 2015	Western Europe	1994	8	4-6	4-9
Antics et al. 2013	Lyon	1995	7	20-25	19-21
Schoetter et al. 2015	Western Europe	1998	8	8-12	8-12
Antics et al. 2013	Lyon		8	10-15	
		2000	8	-	18-20
		2001	7-8	-	31-2
			8	-	24-26
		2002	6	-	15-20
	Lyon	2003	6	10-17	-
Antics et al. 2013	Lyon		6	21-29	20-25
	Lyon		7	13-19	12-15
Chaxel et al. 2004	Grenoble		8	1-15	
Schoetter et al. 2015	Western Europe		8	2-13	2-14
	Lyon		8	3-18	
Antics et al. 2013	Lyon	2005	6-7	26-2	-
	Lyon		7	14-20	-
	Lyon	2006	7	18-31	
Schoetter et al. 2015	Western Europe		7	18-27	19-22
Fouillet et al. 2007	France		7	11-28	
		2009	5	-	23-25
			8	-	18-20
Ung et al. 2013	Isère	2010	7	9-17	
CIRE Auvergne 2011	Puy-de-Dome	2011	7	26-28	-
CIRE Auvergne 2011	Puy-de-Dome		8	19-23	18-24
		2012	6	-	28-30
			7	-	25-27
Ung et al. 2013	Isère		8	20-26	19-24
		2014	6	-	8-10

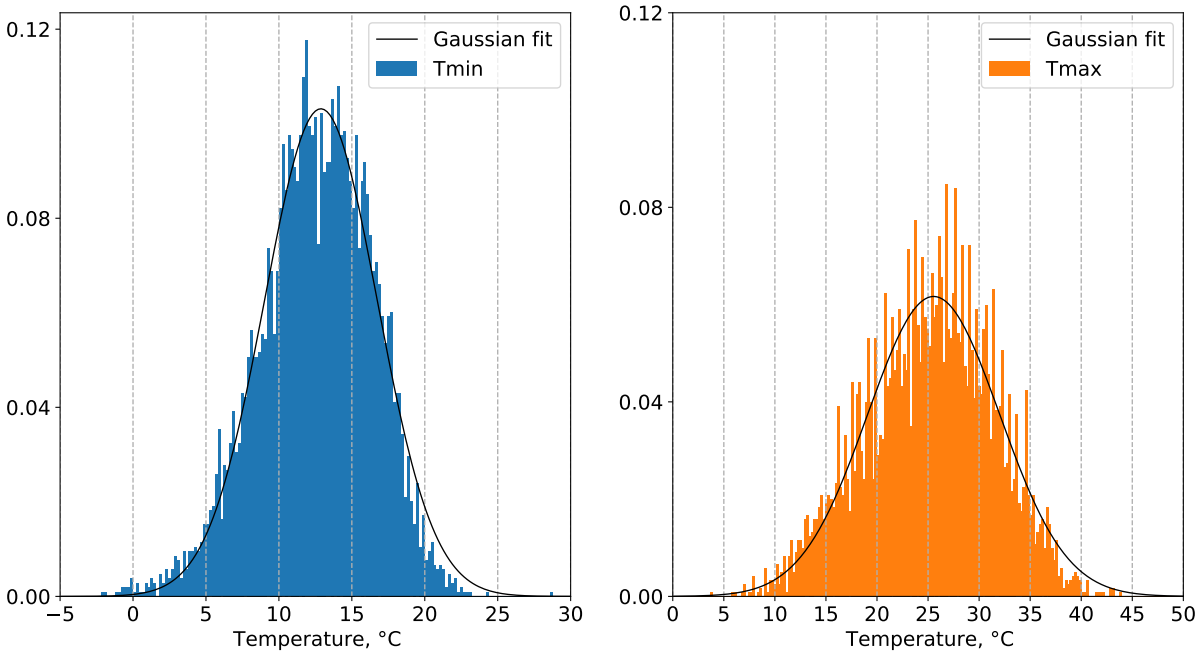

Figure A.3: Histograms of Tmin and Tmax computed for the **observations** taken at the Pont de Claix station for the historical period (1985-2014) and corresponding gaussian fit to the data (black curve).

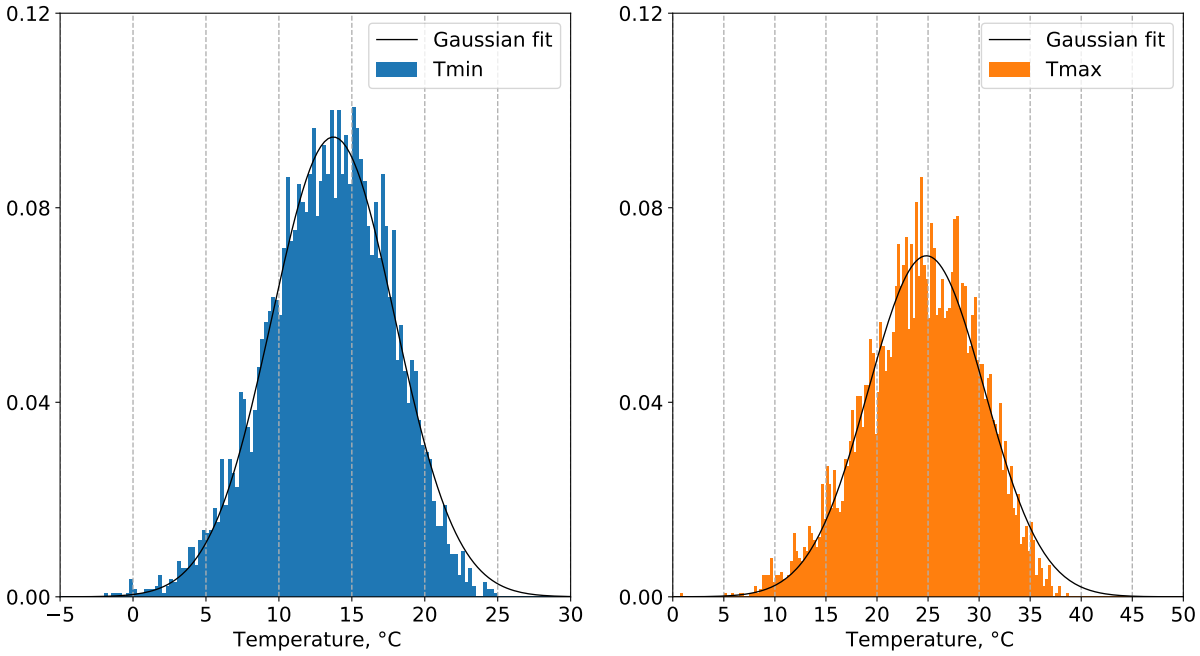

Figure A.4: Histograms of Tmin and Tmax for the **MAR-ERA5 output** for the period 1985-2014 and corresponding gaussian fit to the data (black curve).

Appendix B

Results

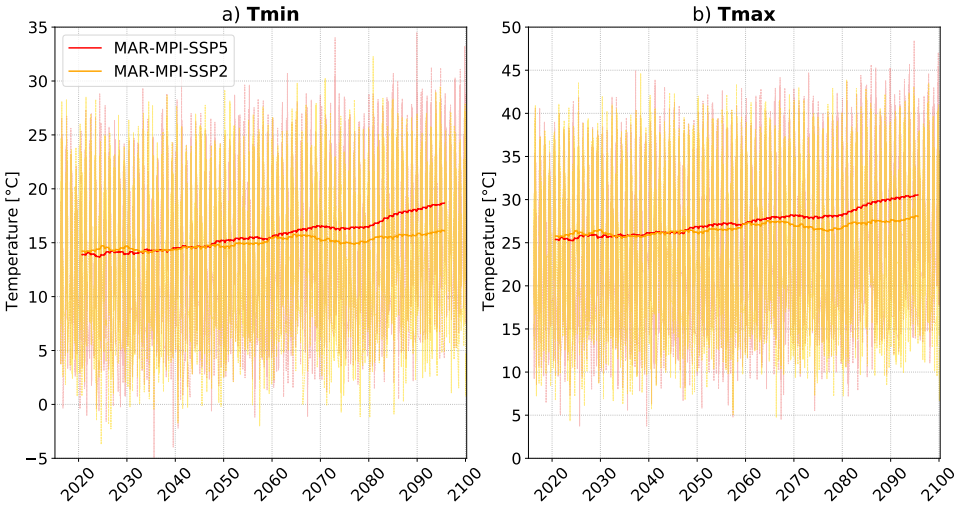

Figure B.1: Time evolution of Tmin and Tmax for MAR-MPI under the SSP2 (orange) and SSP5 (red) scenarios. The solid, bolded lines correspond to a 5 year moving average.

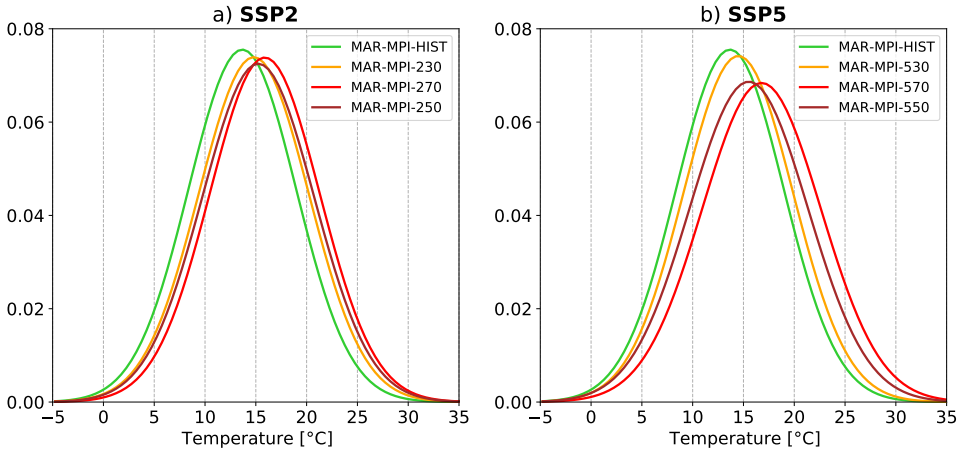

Figure B.2: Gaussian fits of the histograms of MAR-MPI-HIST daily **Tmin** output (green) and for the MAR-MPI daily **Tmin** outputs for the future periods around 2030, 2050 and 2070 (yellow, brown and red, respectively). On the left, the PDFs for the SSP2 scenario and on the right, the PDFs for the SSP5 scenario.

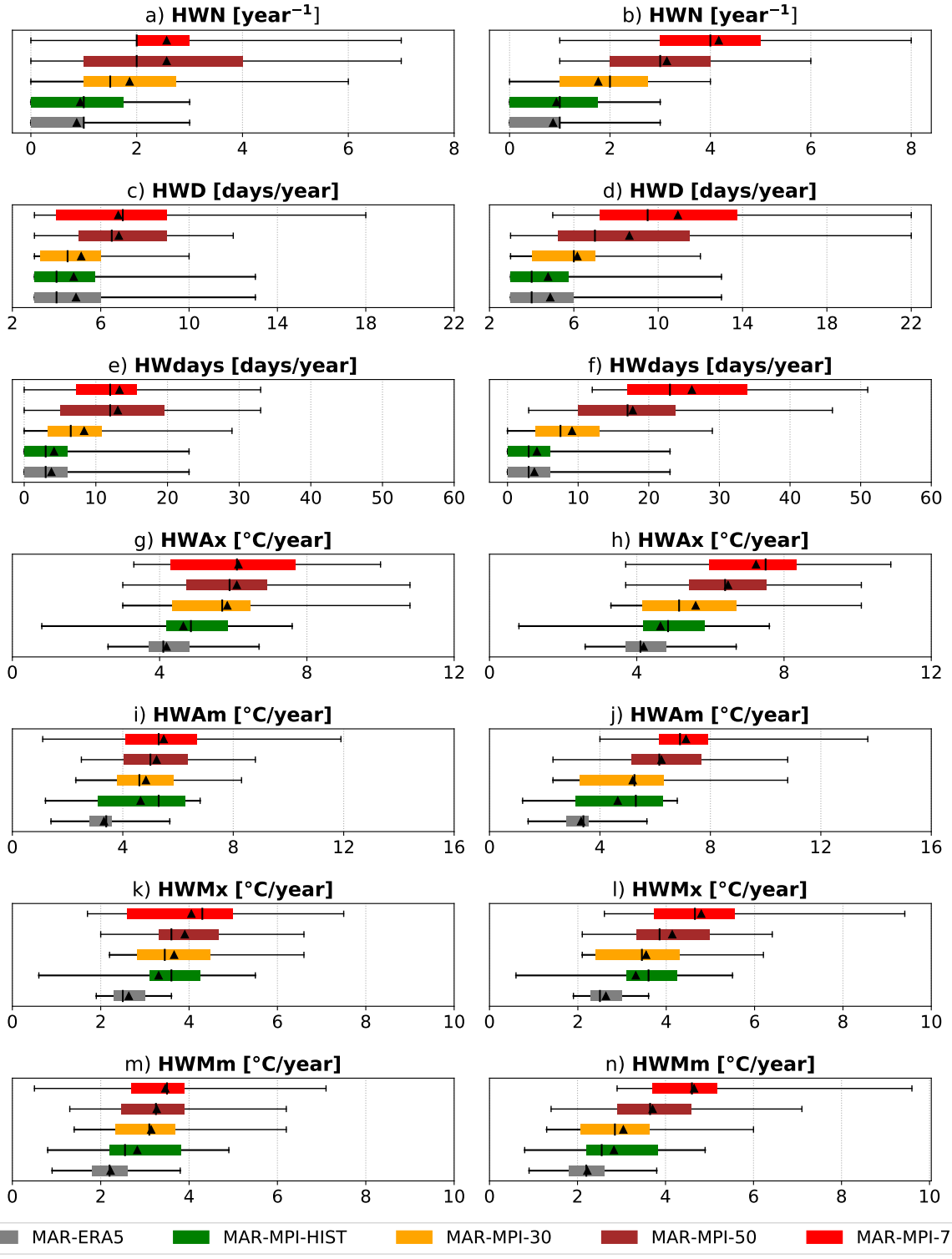

Figure B.3: Yearly HW characteristics averaged over the 30-year periods. The results for MAR-ERA5 (grey) and MAR-MPI (other colors) are displayed as boxplots. The streak indicates the median, the box the interquartile range (i.e. 25th and 75th percentiles), the whisker the full spread (i.e. minimum and maximum values) and the triangle the mean value. Plots on the left column refer to the SSP2 scenario and plots on the right column to the SSP5 scenario.

Appendix C

HWs to be modelled

Table C.1: Dates of hottest HWs found for each scenario found as explained at the end of section 3.3.2. The column "Pct98" indicates the dates of HW defined using the 98th percentile.

SSP2			**SSP5**		
Year-Month	Days	Pct98	Year-Month	Days	Pct98
2038-07	19-24	20-22	2033-06	26-28	26-28
2040-07	12-14	12-14	2037-08	07-09	07-09
2052-07	05-14	10-13	2043-07	16-19	17-19
2058-07	11-17	12-14	2062-07	14-18	14-16
2069-07	23-25	23-25	2062-07/08	20-03	31-03
2078-07/08	18-02	27-30	2063-07	20-24	22-24
2081-06/07	26-04	29-03	2063-08	13-17	14-17
			2073-07	23-27	24-27
			2084-06	14-18	15-17

Appendix D

Gaussian fits

In tables D.1 and D.2, the statistical information for all the data involved in this report and respective Gaussian fits can be found. For the data, the mean, standard deviation and percentiles are computed directly. For the Gaussian fits the mean and standard deviation are parameters intrinsic to the curve fit. These are computed using the Python function *scipy.optimize.curve_fit*[1] with a Gaussian function. The percentiles are computed as in the following example. Let $\mu = 25.6°\text{C}$ and $\sigma = 6.5°\text{C}$ be the mean and standard deviation of a Gaussian fit, respectively. We have to compute the 92nd percentile. First, we need to find the z-score associated to this percentile. The z-score is the value z_p that solves the equation:

$$P(Z < z_p) = 0.92. \tag{D.1}$$

The value of z_p that solves the equation above cannot be found directly, it is solved either by looking at a standard normal distribution table or by approximation. We find that the solution is $z_p = 1.405$, because from the normal table we see that

$$P(Z < 1.405) = 0.92. \tag{D.2}$$

Then, the percentile we are looking for is computed using the following formula:

$$P_{92} = \mu + z_p \cdot \sigma, \tag{D.3}$$

which yields $P_{92} = 34.733°\text{C}$.

[1] *https://docs.scipy.org/doc/scipy/reference/generated/scipy.optimize.curve_fit.html*

Table D.1: Statistical information for all data involved in this project and respective Gaussian fits for **Tmin**.

	Mean	Standard deviation	Percentile 92	Percentile 98
Pont de Claix	12.6	3.9	17.8	19.7
Gaussian fit	13.0	3.9	18.5	21.0
MAR-ERA5	13.5	4.1	19.2	21.2
Gaussian fit	13.7	4.2	19.6	22.3
MAR-MPI-HIST	13.4	5.1	20.4	22.7
Gaussian fit	13.7	5.3	21.1	24.6
MAR-MPI-230	14.3	5.2	21.3	23.9
Gaussian fit	14.8	5.4	22.4	25.9
MAR-MPI-250	14.8	5.2	22.0	24.3
Gaussian fit	15.2	5.5	22.9	26.5
MAR-MPI-270	15.3	5.2	22.2	24.7
Gaussian fit	15.9	5.4	23.5	27.0
MAR-MPI-530	14.1	5.2	21.2	23.9
Gaussian fit	14.5	5.4	22.1	25.6
MAR-MPI-550	15.1	5.5	22.5	25.0
Gaussian fit	15.5	5.8	23.6	27.4
MAR-MPI-570	16.2	5.6	23.8	26.0
Gaussian fit	16.8	5.8	25.0	28.7

Table D.2: Statistical information for all data involved in this project and respective Gaussian fits for **Tmax**.

	Mean	Standard deviation	Percentile 92	Percentile 98
Pont de Claix	25.1	6.2	33.8	36.9
Gaussian fit	25.6	6.5	34.7	38.9
MAR-ERA5	24.4	5.6	31.9	34.6
Gaussian fit	24.8	5.7	32.8	36.5
MAR-MPI-HIST	24.8	6.6	33.8	36.6
Gaussian fit	25.4	7	35.2	39.8
MAR-MPI-230	25.9	6.7	34.9	37.8
Gaussian fit	26.7	7	36.5	41.1
MAR-MPI-250	26.5	6.7	35.6	38.4
Gaussian fit	27.1	7.1	37.1	41.7
MAR-MPI-270	27	6.7	35.7	38.8
Gaussian fit	27.9	6.9	37.6	42.1
MAR-MPI-530	25.7	6.7	34.8	37.8
Gaussian fit	26.3	7.1	36.3	40.9
MAR-MPI-550	26.7	7	36.1	39
Gaussian fit	27.4	7.4	37.8	42.6
MAR-MPI-570	27.9	7	37.3	40
Gaussian fit	28.8	7.3	39.1	43.8